

A Molecular Dynamics Study to Understand Behavior of Corrosion Inhibitors in Bulk
Aqueous Phase and Near Metal-Water Interface

A thesis presented to
the faculty of
the Russ College of Engineering and Technology of Ohio University

In partial fulfillment
of the requirements for the degree
Master of Science

Yathish Kurapati

May 2018

© 2018 Yathish Kurapati. All Rights Reserved

This thesis titled
A Molecular Dynamics Study to Understand Behavior of Corrosion Inhibitors in Bulk
Aqueous Phase and Near Metal-Water Interface

by
YATHISH KURAPATI

has been approved for
the Department of Chemical and Biomolecular Engineering
and the Russ College of Engineering and Technology by

David Young
Research Professor of Chemical and Biomolecular Engineering

Dennis Irwin
Dean, Russ College of Engineering and Technology

ABSTRACT

KURAPATI, YATHISH, M.S., May 2018, Chemical Engineering

A Molecular Dynamics Study to Understand Behavior of Corrosion Inhibitors in Bulk Aqueous Phase and Near Metal-Water Interface

Director of Thesis: David Young

In industry, use of corrosion inhibitors is considered to be an economical and effective way for mitigating corrosion. Despite their impact on reducing corrosion costs, selection of corrosion inhibitors is mostly based on trial-and-error experimentation as molecular-level phenomena underpinning their behavior are poorly understood. In the present work, aggregation and adsorption characteristics of imidazolinium-type model corrosion inhibitors are studied using molecular dynamics (MD). The effect of hydrophobic alkyl tail length on diffusion properties and on micelle formation was investigated using atomistic simulations. Adsorption of an inhibitor molecule at infinite dilution and of a micelle of inhibitor molecules on a metal (Au) surface was investigated by computing free energy profiles of adsorption using Umbrella sampling. Adsorption of single inhibitor molecules was found to be a spontaneous process without any free energy barrier, while the adsorption of a micelle comprised of inhibitor molecules required an external energy of 18 kJ/mole to overcome the free energy barrier.

Keywords: Corrosion inhibitors, Molecular Dynamics, Imidazoline

ACKNOWLEDGEMENTS

I am very grateful to my advisor, Dr. David Young, for all the guidance, support and encouragement I've received over the course of my stay at Ohio University. His faith and confidence in me has been the foundation to all the work herein and his optimistic nature made research work a joyful experience. Thank you very much.

I am deeply indebted to Dr. Sumit Sharma for all the discussions and also for being a driving force behind making this a truly collaborative project. His dedication and scientific rigor continue to be a source of motivation for me. It has been a privilege to witness his passion for scientific questions and his thorough and meticulous approach to research work.

I would also like to thank my thesis committee members Dr. Srdjan Nesic and Dr. David Drabold for their guidance. A special thanks to Dr. Gheorghe Bota, Dr. Win Robbins and Dr. Peng Jin at the Institute for Corrosion and Multiphase Technology (ICMT) for guiding me with my experimental work. I would like to thank the sponsors of the Naphthenic Acid Joint Industry Project (NAPJIP) for their financial support.

I am grateful beyond word to my parents for all the love and support and for always keeping me in their thoughts and prayers. Special thanks to my elder brother Avinash for his unconditional love and for teaching me the meaning of strength in adversity.

Finally, a shout out to all my friends at Ohio University (Sai, Prashant, Rizwan, Surya and Chandu) who kept me relaxed and stopped me from getting lost. I'll always remember the time spent for cricket and movies for years to come.

TABLE OF CONTENTS

	Page
Abstract.....	3
Acknowledgements.....	4
List of Tables	7
List of Figures	8
1 Introduction	12
2 Background.....	17
2.1 Corrosion Inhibitors	18
2.2 Classification of Corrosion Inhibitors.....	18
2.2.1 Inorganic Inhibitors.....	20
2.2.2 Organic Inhibitors	21
2.3 Evaluation of Corrosion Inhibitors.....	22
2.4 Inhibitor Adsorption Mechanisms.....	23
2.5 Corrosion Inhibition Mechanism – A Multiscale Problem	25
2.6 Research Objectives	31
3 Simulation Systems & Methods	33
3.1 Molecular Dynamics	33
3.1.1 Periodic Boundary Conditions.....	36
3.1.2 Potential Truncation.....	37
3.2 Relevant Statistical Mechanics Concepts.....	39
3.2.1 Microstate	39
3.2.2 Ensemble.....	40
3.2.3 Partition Function.....	40

3.2.4	Umbrella Sampling	41
3.2.5	Weighted Histogram Analysis Method (WHAM)	44
3.3	Metrics Used to Characterize the Simulation System	45
3.3.1	Radial Distribution Function (RDF)	45
3.3.2	Diffusion Coefficient Using Mean Squared Displacement	46
3.3.3	Gyration Tensor	47
3.4	Simulation System to Study Aggregation Behavior in Bulk Aqueous Phase	48
3.5	Simulation System to Generate Free Energy Landscapes of Adsorption	54
4	Results & Discussion	58
4.1	Diffusion as a Function of Concentration and Hydrophobicity	58
4.2	Diffusion as a Function of Cluster Size and Hydrophobicity	60
4.2.1	Local Structure of the Liquid Using Radial Distribution Function, $g(r)$	75
4.3	Free Energy Landscapes of Adsorption of an Inhibitor at Infinite Dilution	77
4.4	Free Energy Landscapes of Adsorption of an Inhibitor Cluster	82
5	Conclusions & Future Work	90
5.1	Summary of Results	90
5.2	Future Work	91
	References	93

LIST OF TABLES

	Page
Table 1: Partial charges with hydrogens summed into heavier atoms for imidazolinium ring and pendant group; atom positions labelled in Figure 11.....	51
Table 2: Average of partial charges from Table 1.....	51
Table 3: Free energy, enthalpy and entropy changes on adsorption in an infinite dilution system.	82

LIST OF FIGURES

	Page
Figure 1: Typical three-part structure of a generic imidazolinium-type inhibitor.	22
Figure 2: Schematic showing synergistic effect of anionic species in adsorption of positively charged inhibitors on a positively charged metal surface.	25
Figure 3: Schematic showing how various molecular simulations can be used to understand processes at different length and time scales.	31
Figure 4: Schematic showing the periodic boundary conditions imposed on the simulation box (colored in yellow).....	37
Figure 5: Spherical cut-off shown schematically in an infinite periodic system.....	38
Figure 6: Schematic showing the trajectory of a simulation system from one microstate to another; t_1, t_2, \dots, t_n represent different time steps.....	39
Figure 7: Schematic showing the phase space; $6N$ dimensional volume defining the momentum and position of all particles, N , in the system.....	40
Figure 8: Radial distribution function of SPC/E water.....	46
Figure 9: Schematic showing electron delocalization on the imidazoline ring on accepting a proton	49
Figure 10: Structure of the two imidazolinium derivative molecules (Imid-10 & Imid-17) that are employed in the simulations	50
Figure 11: Imidazolinium ring along with the pendant group. C1, C2, C3, C4, C5, N1, N2, N3 & H1 are only references to particular position.....	51
Figure 12: Snapshot of a typical MD simulation that is used for studying aggregation and diffusion properties; blue represents alkyl tail, red represents hydrophilic head, orange represents chlorides and maroon represents water molecules.	53
Figure 13: Density profile of water in the presence of a metal surface as a function of distance from the metal surface	55
Figure 14: Snapshot of a MD simulation system that is used to study adsorption.	56

Figure 15: Diffusion coefficient of imidazolinium-type corrosion inhibitors as a function of concentration and hydrophobicity (tail length).	58
Figure 16: System spanning cylindrical micelle formed by Imid-17 inhibitors at 0.9M concentration. Water molecules and chlorides are not shown in this snapshot. Periodic images of cluster are shown along the x-axis to visualize the infinite micelle.....	59
Figure 17: Effect of cluster size/aggregation number and hydrophobicity on diffusion coefficient of imidazolinium-type corrosion inhibitors.	61
Figure 18: Effect of hydrophobicity on root mean squared radius of gyration (R_g) of clusters with different aggregation numbers.	62
Figure 19: Shape factors calculated using Eigen values of gyration tensors for different clusters; asphericity and acylindricity are shown as a function of cluster aggregation number and hydrophobicity.	63
Figure 20: Eigen values of gyration tensors for different clusters;.....	65
Figure 21: Diffusion coefficients of Imid-10 clusters calculated from the Stokes – Einstein relationship.....	66
Figure 22: Diffusion coefficients of Imid-17 clusters calculated from the Stokes – Einstein relationship.....	66
Figure 23: Snapshot of different sized clusters formed by Imid-10 molecules; red indicates hydrophilic head and cyan indicates alkyl tail: (a) 8 molecules; (b) 14 molecules; (c) 22 molecules; (d) 32 molecules;	68
Figure 24: Snapshot of different sized clusters formed by Imid-17 molecules; red indicates hydrophilic head and cyan indicates alkyl tail: (a) 8 molecules; (b) 14 molecules; (c) 25 molecules; (d) 32 molecules;	69
Figure 25: Radial distribution of atoms in a cluster w.r.t center of mass of cluster. ‘Hydrophilic’ refers to atoms on the imidazolinium ring & pendant group; ‘Hydrophobic’ refers to carbons in the alkyl tail.....	70
Figure 26: Radial distribution of hydrophilic atoms (atoms on the imidazolinium ring & pendant group) w.r.t. center of cluster	71
Figure 27: Radial distribution function of water w.r.t. terminal carbon as a function of cluster size.....	72

Figure 28: Schematic showing how inhibitor molecules move out from the center of mass to accommodate more molecules and ultimately form a perfect spherical micelle.....	73
Figure 29: Radial distribution of water w.r.t. terminal carbon in alkyl tail, comparison between Imid-10 and Imid-17 clusters.	74
Figure 30: Radial distribution of hydrophobic and hydrophilic atoms w.r.t. center of mass of cluster, comparison of imid-17 & imid-10 clusters having 32 molecules.....	75
Figure 31: Radial distribution function, $g_{OO}(r)$, of SPC/E water.....	77
Figure 32: Radial distribution functions of chloride ions, $g_{H+ - Cl}(r)$, & $g_{Cl - O}(r)$...	77
Figure 33: Histograms generated for Imid-10 by restraining the center of mass (of inhibitor) at different distances from the metal surface	79
Figure 34: Histograms generated for Imid-17 by restraining the center of mass (of inhibitor) at different distances from the metal surface.	80
Figure 35: Free energy profile of Imid-10 and Imid-17 in an infinite dilution system; free energy is represented in terms of thermal energy ($1 kBT = 2.5 kJ/mole$).....	80
Figure 36: MD trajectory of an NVT simulation that has a single cluster of imid-17 inhibitors near the metal surface; orange represent metal (Au) atoms, red represents atoms on hydrophilic head groups and yellow represents hydrophobic alkyl tails. (chlorides and water are not shown for simplicity).	84
Figure 37: Free energy profile of adsorption of Imid-17 cluster (19 molecules) on a Au metal surface	86
Figure 38: Free energy profile of adsorption of Imid-10 cluster (18 molecules) on a Au metal surface.	86
Figure 39: Snapshot of the Imid-17 cluster when the center of mass of cluster is biased at 11\AA from the metal surface. Chlorides not shown for simplicity.....	88
Figure 40: Snapshot of the Imid-10 cluster (plane view) when the center of mass of the cluster is biased at 10\AA from the metal surface. Water not shown for simplicity; red represents hydrophilic head group while cyan represents the hydrophobic tails.....	88
Figure 41: Side view of the Imid-10 cluster shown in Figure 40	89

Figure 42: Minimum free energy state for an Imid-17 cluster; snapshot taken from an unbiased simulation. Blue represents chlorides, yellow represents alkyl tails and red represent polar head groups. 89

1 INTRODUCTION

Corrosion is defined as the degradation of materials, with consequent diminution of their properties, due to deteriorative interactions with environments to which they are exposed [1]. Like natural disasters, corrosion causes huge economic losses, environmental risks, and threatens human life. In a study conducted by NACE, the global cost of corrosion is estimated to be US\$2.5 trillion; this is equivalent to 3.4% of the world's gross domestic product (GDP) (2013) [2]. It is tragic, but at the same time relieving, to know that savings of up to 35% of the cost of corrosion could be realized by using available corrosion control practices [2]. In addition to substantially reducing economic costs, corrosion control is critical to public safety and the environment.

The most commonly used corrosion control strategies include corrosion resistant alloys, protective coatings, corrosion inhibitors, and cathodic protection. Of these control strategies, protective coatings and cathodic protection helps in controlling external corrosion (atmospheric/soil corrosion) of underground pipelines, storage tanks, bridges, and offshore structures. In the chemical, oil, and gas industries, fluids can contain corrosive species which internally degrade processing equipment and pipelines. Use of corrosion resistant alloys (CRAs) is a good choice to reduce internal corrosion but can involve huge capital costs. In addition, use of CRAs can be unfeasible for pre-existing infrastructure. Industry has long considered the use of corrosion inhibitors as an economical and effective way of mitigating internal corrosion. Corrosion inhibitors are heavily utilized in oil and gas production, power industries and water treatment plants [3]. Due to the large commercial market for corrosion inhibitors, estimated to be \$2.5 billion in 2017 for the USA alone [4],

there is a competitive drive to develop new and more efficient formulations. This research is focused primarily on corrosion inhibitors used in the oil and gas industry, however, the lessons learnt can be applied to steel reinforced civil structures and power plants given that corrosion inhibitors are used in improving their lifespans.

Corrosion inhibitors, as defined by Papavinasam [5], are “chemical substances which, when added in small concentrations (ppm) to an environment, minimizes or prevents corrosion”. The inhibition mechanism is typically illustrated by adsorption of inhibitors on the metal surface and formation of self-assembled monolayers (SAMs) [5], [6]. Most of the corrosion inhibitors employed in the oil and gas industry are organic molecules because of their compatibility with hydrocarbon fluids. Typically the inhibitors contain one or more organic functional groups with one or more heteroatoms such as S, P, O or N that are believed to play a critical role in adsorption [5], [7]. Currently, molecules belonging to different chemical families are used as corrosion inhibitors based on application. e.g., fatty acids [8], pyridines [9], [10], imidazolines [11], [12], [13], quaternary ammonium salts, phosphate esters, thiols and 1,3-azoles. Although there are wide varieties of proven corrosion inhibitors, their selection is primarily based on trial-and-error experimentation due to poor knowledge of the underlying molecular phenomena in environments into which they are introduced. Furthermore, for the sake of asset integrity and reducing the impact of industry practice on health, safety and environment, it is of paramount importance to develop science-based models for assessing and predicting the performance of existing/new inhibitors that can be deployed. For these reasons,

understanding the fundamentals of corrosion inhibition mechanisms has been an intensive area of research for the past several decades.

Inhibitor molecules frequently have a three part molecular structure consisting of a hydrophilic head (polar functional groups such as imidazoline, thiol or amine), a hydrophobic tail (saturated (alkyl) or unsaturated), and a pendant group; the latter has been postulated to provide fine-tuning of the interaction of inhibitor with the metal surface as well as other inhibitor molecules [12], [13], [14]. Inhibition efficiency depends on adsorption properties which, in turn, depend on multiple factors such as temperature, molecular structure [12], [13], type of corrosive medium (affects the transport properties of inhibitors), partial charges on the inhibitor molecule/metal surface, surface microstructure, and uniformity of metal surface (oxides, sulfides and sometimes bare metal itself) [12]. Corrosion inhibition by inhibitors is mechanistically complex, and experimental evidence is difficult to obtain as it is mostly governed by molecular and surface phenomena.

Traditionally, inhibitor performance is assessed by employing experimental methods, such as weight loss assessment, polarization curves, electrochemical impedance spectroscopy and atomic force microscopy (AFM). These experimental methods are effective in determining cause-effect relationships for many factors, but they are time-consuming and expensive [15], [16]. With the advancements in technology and the basic understanding of inhibition mechanisms, computational methods have been introduced for studying corrosion inhibitors. Computational modeling of inhibitors can be used for various purposes such as providing the framework for understanding the science of how

functionality and tail groups influence different aspects of the inhibition process, and also as a tool for designing new inhibitors. The use of quantum chemical studies for inhibitors dates back to 1971 [17]. Since then, many efforts have been made to evaluate inhibitors using quantitative structure-activity relationship (QSAR) models, and also force field simulations to a lesser extent. One means to this end is a data-driven approach that correlates different quantum chemical properties, such as atomic charges, electronegativity, dipole moment, energy gap between filled and unfilled molecular orbitals (E_{HOMO} and E_{LUMO}), against inhibition efficiency [18], [19], [20]. The other extreme is the simulation of inhibitor adsorption using molecular modeling tools that can incorporate dynamics, realistic models for metallic and oxidized surfaces and also simulate encountered electrochemical environments [21], [22], [23]. Data obtained from these computational studies can be used to build a multiscale mechanistic model for inhibitor adsorption.

In this study, Classical Molecular Dynamics simulation techniques are used to simulate the behavior of imidazolium-type corrosion inhibitors in the bulk aqueous environment and near the metal-water interface. The goal is to investigate some of the important aspects of inhibitor mechanisms that are often difficult to probe using experiments, which include the formation of aggregates/micelles, free energy of adsorption, and interaction of inhibitors with counter ions (e.g., chlorides in the case of positively charged inhibitors).

Research performed to investigate ‘aggregation’ behavior of inhibitors in the bulk aqueous phase and ‘adsorption’ behavior on the metal is described in this thesis as follows:

- Chapter 2 reviews the literature on corrosion inhibition phenomena and provides a foundation for understanding the research conducted. Specific research objectives are described towards the end of this chapter.
- Chapter 3 describes the computational techniques employed and discusses the methodologies. Also, different terminologies and techniques used in statistical thermodynamics that are relevant to this research are described in this chapter.
- Chapter 4 deals with the results obtained.
- Chapter 5 concludes the results and proposes future work to better understand corrosion inhibition mechanisms using computational techniques.

2 BACKGROUND

Corrosion is described as an electrochemical process involving anodic (oxidation) and cathodic (reduction) reactions. In acidic environments, hydrogen evolution is the typical cathodic reaction and metal oxidation (to its ion) would be the anodic reaction in every corrosion process.



In basic / neutral environments, oxygen reduction is often the cathodic reaction and is commonly observed as most aqueous solutions are in contact with air. Oxidation of metal results in the formation of corrosion product layers (oxides, hydroxides, sulfides, carbonates, etc.) and/or release of metal ions to aqueous environments [24], weakening the metal/alloy. H^+ ions required for cathodic reactions are supplied by corrosive species such as H_2S , CH_3CO_2H , H_2CO_3 , etc., which are frequently present in oil & gas pipelines. Both cathodic and anodic reactions occur simultaneously and their net rates must be equal to each other otherwise metal would spontaneously become electrically charged, which is clearly impossible. Since the two partial reactions (Equations 2.1 & 2.2) are mutually dependent, it is possible to limit corrosion by decreasing the rates of either reaction. By understanding such fundamental processes, many corrosion inhibition strategies like protective coatings, corrosion inhibitors, corrosion resistant alloys, cathodic protection, sacrificial anodes, etc., have been developed. The scope of the research described in this thesis is limited to corrosion inhibitors.

2.1 Corrosion Inhibitors

A corrosion inhibitor is a chemical substance, or formulation, which confers protection to a metal exposed to a corrosive environment. Industry has long considered the use of corrosion inhibitors to be one of the most economic and efficient ways of mitigating corrosion. Even though, there has been a significant development in technology related to corrosion inhibitors in the past few decades [25], most inhibitors are still developed by empirical experimentation, due to poor understanding of the fundamental science underpinning inhibition mechanisms [24]. Generally, their mechanisms of inhibition have been categorized as:

- i) Inhibitor chemically/physically adsorbs on the metal surface and forms a protective film [12], [26] inhibiting either or both anodic and cathodic reactions.
- ii) Inhibitor acts as an oxidizer and forms a protective oxide film on the base metal. This is for metals that demonstrate active-passive transitions [25].
- iii) Inhibitor acts as a ligand that chelates with metal cations forming insoluble chemical complexes on the metal surface [25], [27].

2.2 Classification of Corrosion Inhibitors

Corrosion inhibitors are generally classified as either inorganic or surface-active compounds that, typically, have structures similar to surfactants. Surfactant molecules are amphiphilic in nature, that is they have both hydrophilic (polar group, the 'head') and hydrophobic (the alkyl 'tail') parts. As mentioned earlier, in aqueous solutions, surfactants can act as inhibitors either due to the physical adsorption or chemical bonding with the metal surface, depending on the characteristics of the metal surface and the change in

overall free energy of the system. The water molecules at the metal-water interface region behave differently from the bulk aqueous phase; the water molecules in this region are expected to be strongly adsorbed to the metal which will non-trivially affect the adsorption process. Hence, for an inhibitor to be efficient, it must displace the water molecules from the metal surface and interact with anodic/cathodic reaction sites to retard the corrosion reactions and cause a barrier for diffusion of water and other corrosive species onto the metal surface. Inhibitor selection is specific in terms of metal, environment, temperature, and permissible concentration range. Different classifications of inhibitors have been proposed in the literature based on their chemical nature (organic and inorganic inhibitors) [28], inhibition mechanism (adsorption, precipitation or passivation) [5], and their use in specific environments (acidic, neutral and basic media) [29]. Of all these types, organic inhibitors (adsorption-type) represent the largest class and are commonly employed in oil and gas production processes because of their compatibility and effectiveness in hydrocarbon-containing environments. In this research, imidazolinium-type inhibitors are chosen to be model compounds because of their widespread use in industry; they have also been heavily researched by academia [11], [12], [13], [30]. This family of inhibitors are proven to be effective in inhibiting corrosion and, hence, are a good choice to understand underlying fundamental mechanisms. A typical three-part structure of a generic imidazolinium-type corrosion inhibitor is shown in Figure 1 (section 2.2.2). Précis for organic and inorganic inhibitors are presented below.

2.2.1 Inorganic Inhibitors

The chemicals in which the active part is an inorganic compound are referred to as inorganic corrosion inhibitors. These can be used to inhibit either anodic or cathodic reactions and, based on their functionality, they are considered as anodic or cathodic inhibitors.

Anodic inhibitors (also called passivation inhibitors) are generally employed in near-neutral solutions where there is a tendency to form corrosion products, such as hydroxides, oxides or salts. These are not readily soluble and hence assist the formation of passivating films that inhibit anodic metal dissolution. Some examples of anodic inorganic inhibitors are nitrates, chromates, molybdates, silicates, and phosphates [5].

Cathodic inhibitors work by either retarding the cathodic reaction rate or by precipitating selectively on the cathodic reaction sites; these are referred to as cathodic poisons and cathodic precipitators, respectively. Cathodic precipitators form a barrier of insoluble precipitates over the metal, hence restricting accessibility to corrosive species. Examples are magnesium, zinc and nickel ions that form insoluble hydroxides in water.

Inhibitors based on chromates and arsenic compounds are highly toxic, posing environmental and safety hazards. Strict laws have been imposed internationally to reduce their use which, in turn, increases the need for development of alternative environmentally friendly corrosion inhibitors. This is all the more reason to have improved understanding of inhibition mechanisms.

2.2.2 Organic Inhibitors

Almost 80% of the inhibitors that are employed today are organic compounds that are referred to as ‘mixed’ inhibitors, meaning they are postulated to inhibit both anodic and cathodic reactions. Their efficiency is presumed to be dependent on how well they adsorb and cover the metal surface. However, their actual mode of action, either on cathodic or anodic reactions, is in reality poorly understood [5]. Organic corrosion inhibitors possess at least one functional group, containing a heteroatom such as N, O, P or S, that acts as a reaction center; adsorption strength depends on the charge on this reaction center [31]. Other atomic centers present and structure of the molecule also plays a critical role in determining adsorption efficiency by influencing charge density on the anchor group and promotion of secondary bonding interactions between tails, thereby assisting in formation of self-assembled monolayers (SAMs) [12], [13], [26]. Some of the commonly used organic inhibitors include imidazolines, pyridines, thiols, amines, and 1,3-azoles. More discussion of inhibitor adsorption mechanisms is presented in section 2.4.

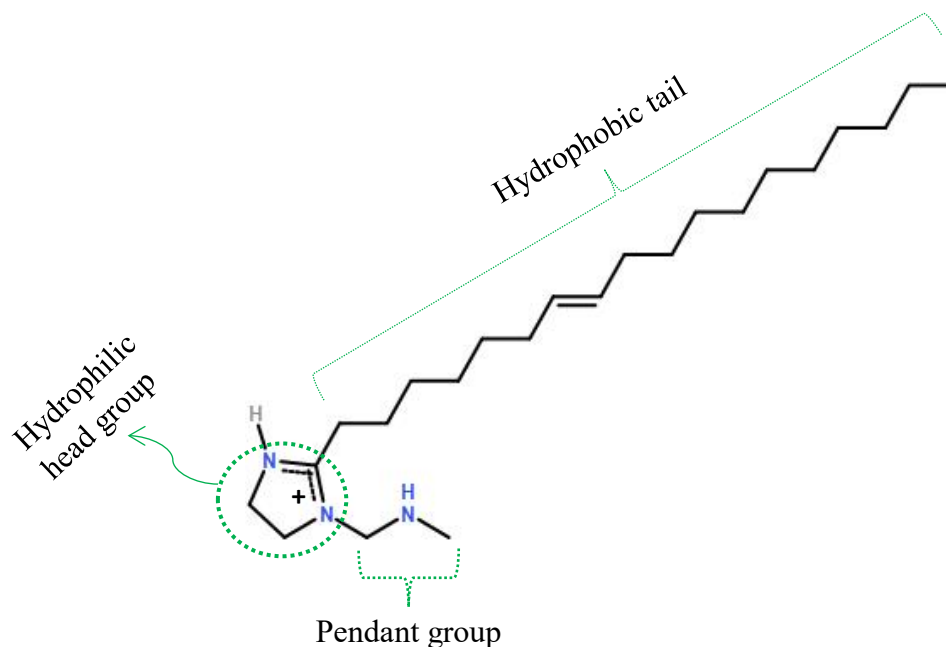


Figure 1: Typical three-part structure of a generic imidazolium-type inhibitor.

2.3 Evaluation of Corrosion Inhibitors

Corrosion inhibitors are mostly evaluated by measuring their corrosion inhibition efficiency [8], which gives the extent of reduction in corrosion rates due to the presence of inhibitor:

$$\eta = \frac{CR_u - CR_i}{CR_u} (* 100\%) \quad (2.3)$$

Where η is the corrosion inhibition efficiency, CR_u is the corrosion rate without inhibitor and CR_i is the corrosion rate in the presence of inhibitor. The corrosion rate is obtained either by linear polarization resistance measurements or impedance spectroscopy measurements for obtaining the active surface area [32], [33], [34].

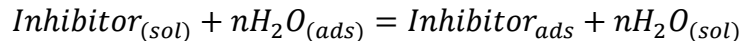
Recently, predicting the efficiency of corrosion inhibitors from theoretical studies has gained momentum due to the advances in technology which facilitate molecular quantum mechanical calculations [35]. Certain quantum chemically derived parameters

such as atomic charges, molecular orbital energies, dipole moments, total energy, etc., are used as measures to predict inhibitor efficiency. This data driven approach is known as QSAR: quantitative structure activity relationships [18], [19]. The challenge to the QSAR approach is that the inhibition efficiency is a function of several other parameters such as surface characteristics, pH, temperature and speciation. Hence, a more comprehensive multiscale mechanistic model is required to predict inhibition efficiency from theoretically derived molecular descriptors.

2.4 Inhibitor Adsorption Mechanisms

The basic premise of inhibition is that the organic inhibitor molecules adsorb (physical adsorption or chemisorption) on the metal surface and block the reaction sites, reducing the available surface area for corrosion and so reducing the corrosion rate [36]. Physisorption is primarily due to electrostatic interactions between the inhibitor molecule and the metal surface; charges play a critical role in this phenomenon. Certain counter ions like halide / acetate ions, in the case of positively charged metals, are known to provide synergistic effects that promote corrosion inhibition, Figure 2. However, physical adsorption is a dynamic, reversible process where desorption of inhibitor molecules is generally favored with an increase in temperature. Chemisorption, on the other hand, is more effective as it involves orbital interactions (electron cloud interaction) between the inhibitor molecule and the metal, however, the kinetics of chemical adsorption is slow. Certain inhibitor molecules, e.g., acetylenic molecules, may undergo surface reactions forming polymeric films which reduce the available surface area for corrosion.

In generic terms, adsorption of the inhibitor molecules is expressed as:



Where n is the number of water molecules displaced from the metal surface for each molecule of inhibitor adsorbed. It is logical to assume that the value of n depends on the cross-sectional area of the inhibitor with respect to that of the water molecule. The above explained process is generic and classification of inhibitors based on specific adsorption mechanisms has been described by Lorenz [37] in terms of geometric blockage, active-site blockage, and electro-catalytic effects.

a. Geometric Blocking Inhibitors: Geometric blocking refers to the reduction of surface area (available for electrochemical reactions) due to the adsorption of electrochemically inactive and non-reducible species. The mechanisms of the electrochemical reactions, the open circuit potential, and the polarization curves remain unchanged. Therefore, this mechanism assumes that corrosion inhibition efficiency, η , is directly related to the fraction of metal surface covered by inhibitors, θ [38], [39].

$$\eta \propto \theta$$

b. Active-site Blocking Inhibitors: The region of the metal surface where electrochemical reactions occur are referred to as active sites. Active-site blocking inhibitors retard reactions associated with either anodic or cathodic processes [5]. Cathodic inhibitors retard the cathodic reaction by blocking or precipitating selectively on cathodic areas, limiting the transport of reducible species to the surface. Anodic inhibitors force the metal surface into the passivation region, by causing a large anodic shift in the open circuit potential. The usage of these inhibitors is specific to those which have a passivation behavior when they are anodically polarized.

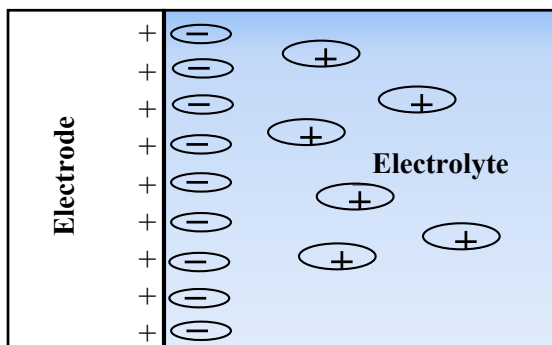


Figure 2: Schematic showing synergistic effect of anionic species in adsorption of positively charged inhibitors on a positively charged metal surface.

c. Electro-Catalytic Inhibitors: Electro-catalytic inhibitors affect the average activation energy barriers of the electrochemical (either or both cathodic and anodic) reactions associated with corrosion processes [39]. This change in the activation energy alters the nature of the species that form during the corrosion process, potentially leading to the development of a passive surface layer or a change in the mechanism of corrosion reactions [29]. Consequently, electrochemical behavior can change radically [39]. In potentiodynamic polarization, a change in Tafel slope is the evidence for this type of inhibition.

2.5 Corrosion Inhibition Mechanism – A Multiscale Problem

From the discussion earlier, it is evident that corrosion inhibition is a complex phenomenon involving many distinct processes ranging from electron-cloud interactions ($\sim 10^{-10}$ m) to large scale processes such as self-assembly and associated with phase transitions ($\sim 10^{-6}$ m). In the past decade there has been tremendous advancements in technology and with the available computational resources, it is possible to study

multiscale problems, such as corrosion inhibition, using computational techniques. Different techniques are used at various length and time scales to obtain different kinds of information (see Figure 3). The central idea is to deconstruct such a multiscale problem into sub-processes, understand each using various experimental & computational techniques, and finally stitch all the information together to advance building a multi-physics, multiscale model. This concept was put forward by Taylor, *et al.*, to study corrosion inhibition phenomena [40]. Currently, the amount of data generated on corrosion inhibition is very limited and there still exists many knowledge gaps. Mechanisms of corrosion inhibition are elucidated using domain and micro process approaches to gain a better insight on knowledge gaps and where a particular technique can be applied. Most of the following information reviewed and discussed below is taken from Taylor, *et al.*, [40].

Macroscopic bulk phase characteristics, near-surface environment that involves the mass-transport layer and the metal-water interface, dominated by the microstructure and passive layers of corrosion products were identified as three key domains. Each of these domains have specific processes occurring simultaneously that influence the inhibition efficiency.

a. Speciation: When corrosion inhibitor is introduced into the aqueous phase, it undergoes equilibration through a set of interactions with water, which include protonation and molecular aggregation (micelle formation). As mentioned earlier, inhibitor molecules typically contain one or more functional groups that accept or donate H^+ . This tendency is described by the acid dissociation constant (pK_a) and is dependent on pH of the solution. Another thermodynamically favored interaction is micellization; micelle formation

requires that the inhibitor concentration is above the critical micelle concentration (CMC) and overall free energy of the system decreases. Once inhibitor concentration exceeds CMC, no further inhibition action is promoted as any additional molecules will lead to formation of micelles in the bulk solution [41]. Therefore, CMC is an effective boundary condition below which inhibitor adsorption is likely to be efficient. Hence, a clear understanding of factors affecting CMC and aggregation of molecules is essential for establishing corrosion inhibition mechanisms. CMC's can be measured using experimental techniques including surface tension measurement and light scattering experiments. Computational techniques such as Dissipative particle dynamics simulations were also used to estimate CMC [42].

b. Partitioning: Typically, the corrosive environment encountered in oil and gas production involves mixed phases of hydrocarbons and water. Most of the inhibitors, being organic in nature, have a propensity to segregate into the hydrocarbon phase. This behavior is measured in terms of partition coefficients, $\log P$, where P denotes the equilibrium constant for the concentration of inhibitor in the hydrocarbon phase *versus* the aqueous phase. Hence, the effective concentration of inhibitor available for adsorption is dependent on its partitioning behavior. It is possible to calculate partition coefficient using first principles quantum calculations [43].

c. Multiphase flow: Inhibitor molecules are typically surfactants that have the ability to modify oil/water, oil/metal, and water/metal interfaces. Flow velocity and the amount of water present could possibly affect the ability of inhibitors to modify surfaces. The inhibitors are known to reduce oil/water interfacial tension and increase oil wettability of

the metal surface [44]. This ability of inhibitors to lower interfacial tension make them good emulsifiers, but emulsification with water has to be avoided as water needs to be separated downstream. Also, flow affects the concentration profile of the inhibitor from bulk to the metal surface over time. The main parameters involved here are the oil/water interfacial tension and the oil/metal and water/metal surface energies. These can be calculated using density functional theory calculations.

d. Adsorption: As discussed earlier, inhibition processes are often explained in terms of adsorption; the most studied characteristic of inhibition phenomena. Ramachandran, et al., explained inhibition mechanisms by formation of self-assembled monolayers (SAMs) at the metal/environment interface using quantum calculations and force-field simulations [12]. They postulated that electron donating groups on inhibitors bind strongly to the metal surface / oxides by displacing water, their hydrophobic alkyl tails forming a barrier that retards the diffusion of water and other corrosive species to the metal surface. Various research studies have also focused on identifying the role of molecular structure on adsorption [11], [12], [13]. Here critical parameters such as binding energy, SAM packing efficiency and diffusivity of corrosive species therein can be calculated using Density Function Theory and classical molecular dynamics (MD) / Monte Carlo (MC) simulations. Sophisticated equipment such as atomic force microscopes (AFMs) are also used to study SAMs and bilayer formation. Inhibitor-metal, inhibitor-inhibitor, and solvent-mediated interactions, as well as entropic changes associated with the adsorption process, contribute to the overall adsorption behavior. Along with experiments, molecular simulations can play an important role in identifying these contributions [45].

e. SAM properties, packing efficiency and transport properties: The characteristics of SAMs are expected to be a function of molecular structure (packing efficiency) and competition between inhibitor molecules and other species (water molecules, counter ions, etc.) that influence how corrosive species approach the metal surface. Recent studies using AFM showed formation of bilayers upon adsorption [46]. Formation of these self-assembled structures may be an activated process and hence slow in comparison to timescales wherein corrosion may be observed. Therefore, kinetics of adsorption/desorption and transport properties of water, counter ions, and inhibitor molecules is critical for understanding inhibition mechanisms and inhibitor design. These can be studied using a combination of experimental and classical molecular dynamics simulations.

f. Cathodic and anodic reactions: Corrosion inhibitors interfere with anodic and cathodic reactions thereby affecting electrochemical behavior at the metal surface. The presence of self-assembled structures at this interface will govern transport rates of anions and solvated cations through the SAM. Interaction of inhibitor molecules with point defects in the metal lattice may define long-term corrosion rates [47]. In some environments, inhibitors themselves might cause corrosion, but at a very low rate. Most of these factors are studied using polarization curves and electrochemical impedance spectroscopy techniques. However, many of these phenomena can be predicted using theoretical molecular modeling studies [40], [48].

g. Secondary reactions: Even in the presence of inhibitor there is some corrosion happening and it changes metal atoms to a higher oxidation state which will eventually form precipitates, or at least salts in aqueous solution. Therefore, SAMs not only contain

inhibitor molecules but also may contain entrapped metal ions/complexes. These may improve packing efficiency of SAMs and add to the mass transport barrier that retards corrosion. Also, there can be secondary interactions disrupting SAM formation.

h. Metal surface and role of microstructure: The chemical and structural identity of the exposed metal surface is an essential element in building multiphysics models, after all, inhibitors are used to protect the metal surface. The characteristics of the metal surface are dependent on pH, electrochemical potential, temperature, and the microstructure of the alloy. Mild steel, the most widely studied material in corrosion inhibitor research, has an α -Fe lattice with other trace elements therein, the surface is likely to contain oxides, carbides (as residues), sulfides (e.g., mackinawite, pyrrhotite, pyrite, troilite), carbonates and hydroxides in corrosive environments; present as single or multiple phases depending on the thermodynamics and kinetics of the corrosion reactions.

i. Interaction with inhibitor package and other organics, ions: Most of the commercially available inhibitors are distributed as packages which contain biocides, surfactants, scale inhibitors etc., in precise formulations. There is evidence that halide ions present in brines and frequently present in inhibitor packages have synergistic effects in inhibiting corrosion [49]. Thus, the collective interaction of these compounds in different regions should be considered in the Multiphysics model.

It is evident that inhibition mechanisms encompass numerous micro-processes. In this research, an attempt was made to fill some of the knowledge gaps described above using atomistic simulations.

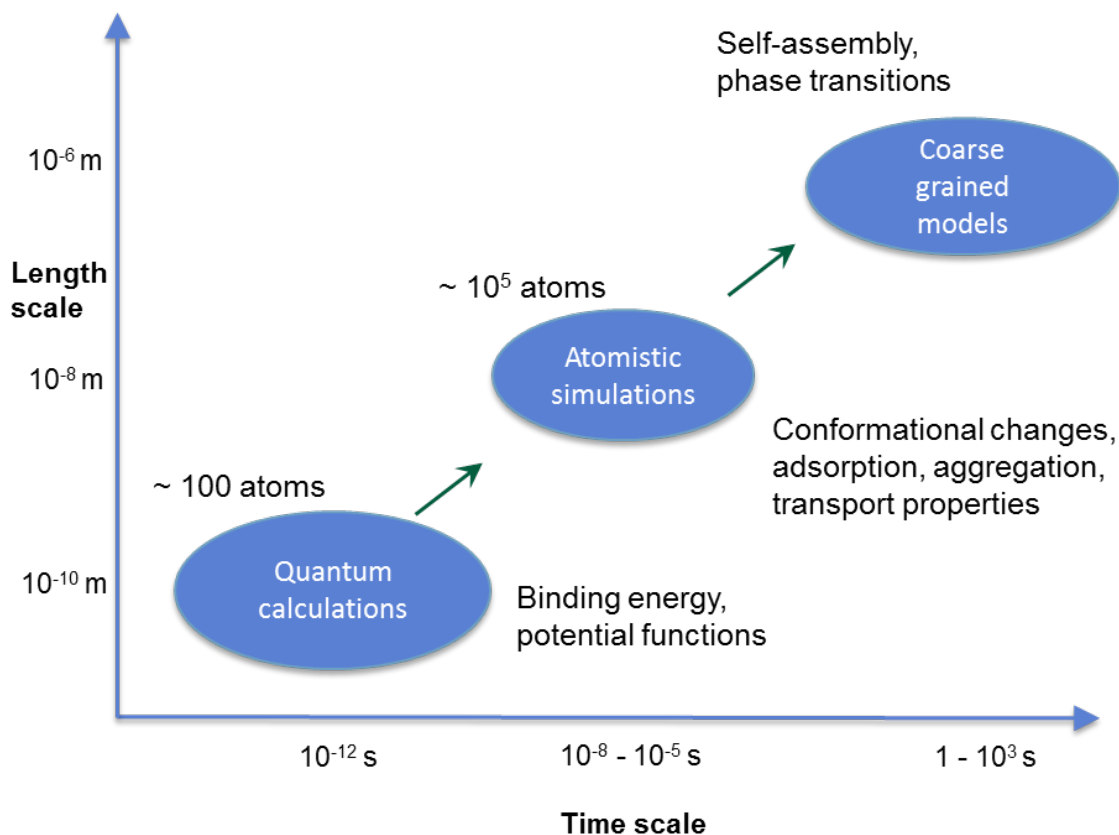


Figure 3: Schematic showing how various molecular simulations can be used to understand processes at different length and time scales.

2.6 Research Objectives

Homologous series of inhibitors have been widely studied [12], [13] by experimental methods, and molecules with longer alkyl tails are often reported to be more efficient inhibitors. However, the real reason for their superior efficiency remains incompletely understood. Longer alkyl tails make molecules more hydrophobic and generally have a higher tendency to form clusters / micelles in the aqueous phase. Also, the hydrophobicity makes the adsorption on the surface more favorable. A single molecule in the bulk aqueous phase can either be a part of micelles or diffuse to the metal surface

and adsorb on the metal. In addition, micelles may diffuse to the surface and adsorb if the latter state is thermodynamically more favorable. Such conclusions are difficult to make purely from experiments. In order to gain better insights on the effect of hydrophobicity on corrosion inhibition, an atomistic simulation technique named classical molecular dynamics is employed in the research discussed in the thesis.

The primary objectives of the research reported herein are as follows:

- i) Study the effect of alkyl tail length of inhibitor molecules on cluster / micelle formation. The size and geometry of clusters are expected to be a function of alkyl tail lengths, which will affect their diffusion and adsorption behavior.
- ii) Study adsorption behavior of an inhibitor molecule in infinite dilution on metal surface; the region at the metal-water interface behaves differently from the bulk aqueous phase. Water is expected to strongly interact with the metal surface, which may non-trivially affect the adsorption.
- iii) Study adsorption behavior of a micelle of inhibitor molecules on metal surface. Due to the presence of inhibitor-inhibitor interactions and electric double layer of the cluster (in case of charged inhibitor molecules), a different adsorption behavior is expected compared to a single inhibitor system.

3 SIMULATION SYSTEMS & METHODS

3.1 Molecular Dynamics

Molecular dynamics (MD) is a modeling technique used to simulate complex systems at the atomic level. Time evolution of the system is studied by solving Newton's equations of motion numerically; the thermodynamic properties of the system (of interest) are derived by conducting various 'computer experiments'. In the past few decades, MD has gained prominence in studying dynamics and structure of biomolecules, such as proteins and nucleic acids. In MD methods, the physical system can be represented using either 'classical' or 'quantum' approaches. In the 'classical' mechanics approach to MD simulations, all atoms are treated as classical particles and the dynamics of the system is governed by laws of classical physics. This is a good approximation as the de Broglie wavelength of atoms is much smaller than their diameter and hence are big enough to be treated as classical particles. In the 'quantum' MD approach, the electron cloud interaction and the quantum nature of the chemical bonds are explicitly taken into consideration (using principles of quantum mechanics). Although quantum MD is more precise and accurate, it is significantly more computationally challenging and hence is nonviable to solve systems consisting of thousands of atoms over timescales of nanoseconds. In this research, a classical MD approach is used and will be referred to as MD from now on.

Assuming atoms to be classical particles, the microscopic state of a system can be completely described in terms of the positions and momenta of its constituent set of particles, *i.e.*, atoms and molecules. The physical systems are typically described as an assembly of atoms kept together by means of interatomic forces; referred to as atomic force

field models. Interactions between atoms are described using ‘potential’ that is only a function of their positions; $U(\mathbf{r}_1, \mathbf{r}_2, \dots, \mathbf{r}_N)$ refers to the potential energy of a system containing N interacting atoms, where \mathbf{r}_i refers to the position vector of i^{th} atom. Knowing the potential energy of the system, the force acting on each atom can be computed by the gradient with respect to atomic displacements. Equation 3.1 gives the force acting upon i^{th} atom:

$$\mathbf{F}_i = -\nabla_{\mathbf{r}_i} U(\mathbf{r}_1, \dots, \mathbf{r}_N) = -\left(\frac{\partial U}{\partial x_i}, \frac{\partial U}{\partial y_j}, \frac{\partial U}{\partial z_i} \right) \quad (3.1)$$

For the simplest case of a system containing N atoms (neutral), the potential energy is given by:

$$U = \sum_i v_1(r_i) + \sum_i \sum_{j>i} v_2(r_i, r_j) + \sum_i \sum_{j>i} \sum_{k>j>i} v_3(r_i, r_j, r_k) + \dots \quad (3.2)$$

The first term in the above equation represents the effect of an external field while the remaining terms account for interparticle interactions. The second term, pair potential, is most significant and is only a function of the interatomic distance, r_{ij} . The contributions from many-body (four and above) interactions is very small and are mostly ignored. Typically, liquid systems are described using effective pair potentials, that include average three-body effects, as it measures liquid properties remarkably well [50] and also conserves simulation time. Simpler, more idealized pair potentials commonly used in computer simulations are the Lennard-Jones potentials:

$$v^{LJ}(r) = 4\varepsilon \left(\left(\frac{\sigma}{r} \right)^{12} - \left(\frac{\sigma}{r} \right)^6 \right) \quad (3.3)$$

Where σ and ϵ are the two parameters that are to be chosen, as appropriate. For ions or atoms with partial charges, Coulombic interactions are also included in the potential term to account for long-range interactions.

For molecules, the potential term is more complicated as one has to incorporate bond and angle potentials as well. In a molecule, nuclei share the electrons that are delocalized resulting in an electronic cloud. Assuming the Born-Oppenheimer approximation, the motion of electrons and nuclei can be separated. The nuclei are considered to move in a field of averaged electron densities; this resulted in the concept of the potential energy surface. It determines the dynamics of the nuclei without considering electrons explicitly. In classical MD, physics and chemistry of the system are mimicked using empirical potentials with a specific functional form. A typical functional form of force field used is given in equation 3.4.

$$U = \sum_{bonds} a_i (l_i - l_{io})^2 + \sum_{angles} b_i (\theta_i - \theta_{io})^2 + \sum_{dihedrals} c_i [1 + \cos(n\omega_i - \gamma_i)] + \sum_{atom\ pairs} 4\epsilon_{ij} \left[\left(\frac{\sigma_{ij}}{r_{ij}} \right)^{12} - \left(\frac{\sigma_{ij}}{r_{ij}} \right)^6 \right] + \sum_{atom\ pairs} k q_i q_j / r_{ij} \quad (3.4)$$

Where the first three terms define the covalent structure of the system and last two terms are the LJ potentials and long-range Coulombic interactions.

Once the appropriate potential is chosen, forces acting on each atom at a given time instant, t , are computed using eq. 3.1 and then using Newton's laws, Equations of motion are solved numerically to find the position and momentum of particles at another time instant, $t+\Delta t$. The Verlet algorithm is frequently used in MD simulations to find positions and velocities because of its simplicity and efficiency [50]. Since trajectories are obtained from numerical integration, the smaller the time step, Δt , the more accurate is the MD

trajectory. However, sometimes larger time steps allow sampling of longer trajectories. Therefore, using MD simulations, the dynamic events that influence the properties of the physical system can be traced at the atomic level.

3.1.1 Periodic Boundary Conditions

MD simulations are generally performed on a limited number of molecules, $10 < N < 10000$, confined to a simulation box. In stepwise numerical integration, positions and velocities of all particles needs to be updated in every timestep. This also means that the force acting on each particle needs to be recomputed every timestep. Thus, time taken is proportional to N^2 , so force/energy calculations inevitably define the speed of the simulation. Hence, it takes less time and is less expensive to simulate a smaller system, but it is important to ensure that the simulation box represents the macroscopic system. One major obstacle with using a simulation box is that the atoms present at a boundary will experience different forces from molecules in the bulk. This issue of ‘boundary effects’ is solved by implementing “periodic boundary conditions”, *i.e.*, the simulation box is replicated throughout the space to form an infinite ‘lattice’. This means that every atom in the simulation box has periodic images which behave exactly the same way as the original one (Figure 4). Thus, as an atom leaves the simulation box from one face, its periodic image will enter the simulation box through the opposite face. Effectively, this means that there are no walls and the problem of boundary effects is eliminated [50].

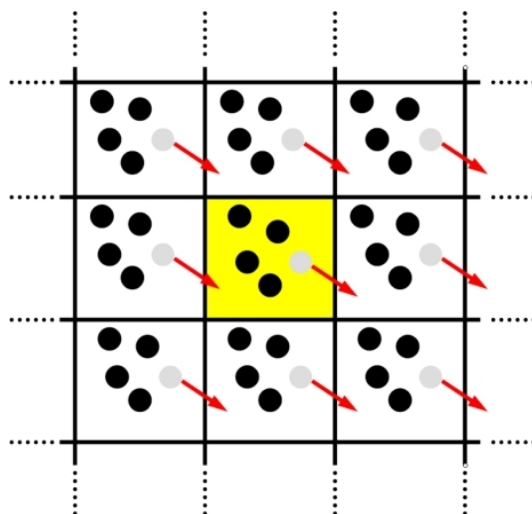


Figure 4: Schematic showing the periodic boundary conditions imposed on the simulation box (colored in yellow).

It is now necessary to ensure that this small, infinitely periodic system is representative of the macroscopic system that is being simulated. It has to be noted that the macroscopic system is not symmetric and, hence, no particle in the simulation system must be able to sense the symmetry introduced in terms of periodic lattices; this will depend on the interatomic potential and the properties being investigated. Hence, dimensions of the simulation box must be chosen in such a way that no atom has any substantial interaction with its periodic image. Typically for a system of Lennard-Jones (LJ) atoms, a simulation box of size $L = 6\sigma$ will work. But for long-range potentials, in the case of ions, special methods like Ewald summation, particle-meshed Ewald methods (PPME) are employed.

3.1.2 Potential Truncation

In a periodic lattice system, to compute net force on an atom, one must consider interactions between this atom and every other atom in the simulation box. In addition, interaction with all the periodic images shall be considered; this becomes an infinite

number of calculations and is practically impossible to compute. Therefore, for a short-range potential like LJ potentials, the interactions are restricted by making an approximation. Consider the atom (of interest) to reside at the center of a region which is equivalent to the original simulation box (same size and shape). The interactions are restricted to only those atoms whose nuclear center lies within that region in relation to the closest periodic images of remaining atoms; this is known as ‘minimum image convention’. Since the simulation box size is chosen to be big enough that it replicates the macroscopic system, this truncation of potential is a good approximation and errors introduced are negligible. Sometimes for large systems, further approximation significantly improves the speed of the simulation without significantly affecting accuracy. The neighbors close to the atom of interest contribute to the major chunk of interactions and, hence, a spherical cut-off is applied (for short-range forces like in LJ systems); see Figure 5. This means we set the pair potential to 0 if $r_{ij} > r_c$. Error introduced due to spherical cut-off depends on r_c and is typically chosen to be less than $\frac{1}{2}L$.

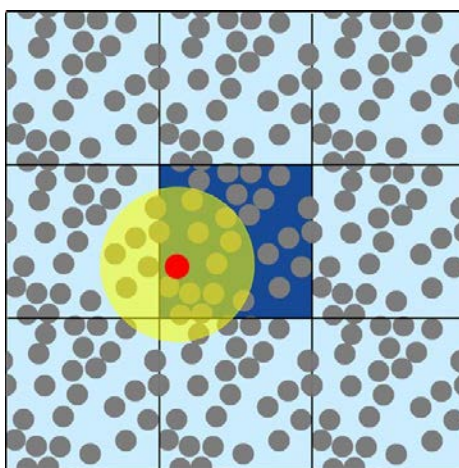


Figure 5: Spherical cut-off shown schematically in an infinite periodic system.

3.2 Relevant Statistical Mechanics Concepts

Statistical mechanics is a means to obtain macroscopic thermodynamic properties from the molecular motions of the constituents of a system. Some statistical mechanics concepts that are employed in this research for doing cluster analysis and generating free energy profiles of adsorption are reviewed in this section.

3.2.1 Microstate

As discussed in the previous section, in MD the system is defined by positions and velocities of all the particles therein. Under specific constraints of pressure, temperature and chemical potential, the positions and velocities of the particles in a system keep changing with time due to the intermolecular forces they exert on each other. Each of these configurations, set of positions and velocities of all the particles in a system is called a microstate, *i.e.*, the microstate can be thought of as a snapshot of the system at a particular time instant. As the system evolves, it goes from one microstate to another as shown in Figure 6. Thus, for a given macroscopic condition, a microstate is represented by a point in phase space, Figure 7, where phase space represents all possible microstates.

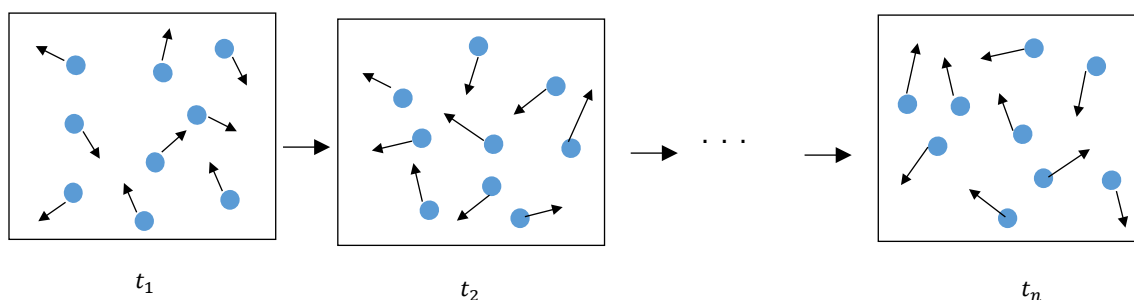


Figure 6: Schematic showing the trajectory of a simulation system from one microstate to another; t_1, t_2, \dots, t_n represent different time steps.

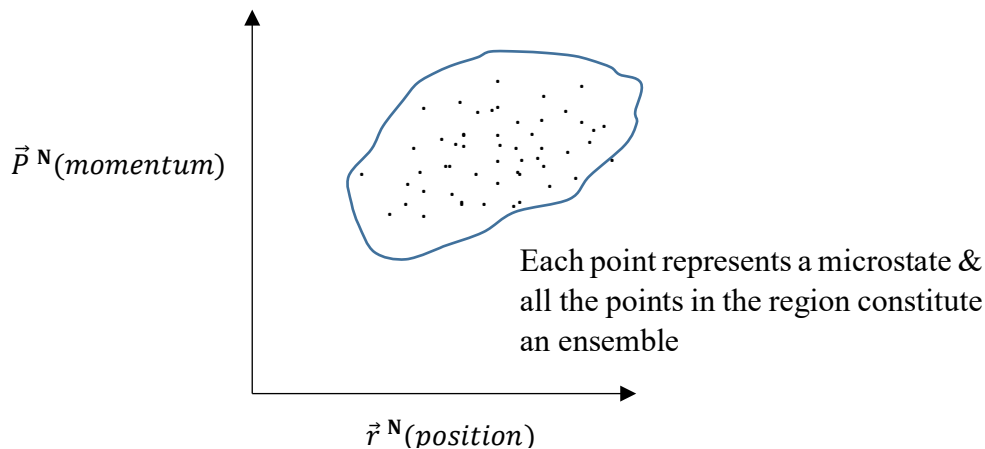


Figure 7: Schematic showing the phase space; $6N$ dimensional volume defining the momentum and position of all particles, N , in the system.

3.2.2 Ensemble

An ensemble is a collection of a large number of microstates of the system under the same macroscopic condition or having the same macro-state. A thermodynamic state is the ensemble average of a large number of microstates of the system. Different types of ensembles are generally used depending on the interaction of the system with the surroundings. In this work, two ensembles are considered, an isothermal-isobaric ensemble (constant N , T and P) to study aggregation in the bulk and a canonical ensemble (constant N , T and V) to study adsorption.

3.2.3 Partition Function

The partition function of an ensemble is a thermodynamic function of state variables, such as temperature and volume, that is used to describe the statistical properties of an ensemble. Most of the thermodynamic properties of a system, such as entropy, free

energy, pressure, etc., can be obtained from a partition function. The canonical ensemble partition function of a system with continuous energy states is given by:

$$Z(T, V, N) = \int e^{-\beta E(\mathbf{R})} d\mathbf{R} \quad (3.5)$$

In this expression above, \mathbf{R} denotes the position vectors of the atoms in the system, $\beta = \frac{1}{k_B T}$ with k_B being the Boltzmann constant and T is the temperature; $E(\mathbf{R})$ denotes the energy of a microstate that depends on the positions and momentum of the particles.

Free energy for a canonical ensemble, A , is given by Equation 3.6.

$$A(T, V, N) = -\frac{1}{\beta} \ln(Z(T, V, N)) \quad (3.6)$$

The partition function gives the probability of finding a system in a particular microstate under specific macroscopic constraints.

3.2.4 Umbrella Sampling

As discussed earlier, most of the corrosion inhibitors are surface-active compounds that are amphiphilic in nature. In polar solvents like water, these molecules has a tendency to agglomerate at interfaces and in the bulk solution. The associated molecules in the bulk (micelles) and the structures formed upon adsorption (for instance self-assembled monolayers) represent entirely different free energy states under the same macroscopic conditions. These different states are possible in the simulation because the system evolves towards a configuration that is lowest in free energy. Since the free energy landscape is unknown beforehand, there are many possible local minima of free energy along a particular reaction coordinate. A *reaction coordinate* is an abstract coordinate that is used to describe the path or progress of a reaction. For instance, distance from the metal surface is considered as reaction coordinate for adsorption processes.

As the simulations are initiated using random configurations, it is most likely that the system reaches an equilibrium at a local minimum and gets kinetically trapped due to the energy barrier(s) involved. In such cases, one does not sample all the microstates in the phase space and hence free energy profiles cannot be generated accurately. To overcome this sampling issue in molecular simulations, many techniques were developed. One of the most popular sampling methods that is used to calculate free energy differences along a reaction coordinate is ‘Umbrella sampling or biased molecular dynamics’ [51].

In umbrella sampling, the system is driven over an energy barrier by modifying the energy expression in order to reduce the barrier (Equation 3.7). The reaction coordinate (ξ) is divided into a number of windows and each window is characterized by a target reaction coordinate, ξ_i , where i represents a window. In each window, a bias potential $V_i(\xi)$, which is only a function of the reaction coordinate, is applied to the system. This will bias the system towards configurations whose reaction coordinate value is close to the ξ_i of that window.

$$U_i^b(\mathbf{r}) = U_i(\mathbf{r}) + V_i(\xi) \quad (3.7)$$

Where, $U_i^b(\mathbf{r})$ is the modified (biased) energy of the system. The quantities without superscripts are always unbiased. In order to generate a free energy landscape along a reaction coordinate, the unbiased probability distribution is required; $P_i^u(\xi)$, along ξ , which is given by Equation 3.8.

$$P_i^u(\xi) = \frac{\int e^{-\beta(U_i(\mathbf{r}))} \delta(\xi - \xi_i) d\mathbf{r}}{\int e^{-\beta(U_i(\mathbf{r}))} d\mathbf{r}} \quad (3.8)$$

MD simulation of this biased umbrella sampling system provides the biased probability distribution along the reaction coordinate, $P_i^b(\xi)$ is given by Equation 3.9.

$$P_i^b(\xi) = \frac{\int e^{-\beta(U_i(r)+V_i(\xi))} \delta(\xi-\xi_i) dr}{\int e^{-\beta(U_i(r)+V_i(\xi))} dr} \quad (3.9)$$

Since the bias potential is dependent only on ξ and the integration in the numerator is performed over all degrees of freedom but ξ , Equation 3.9 becomes Equation 3.10.

$$P_i^b(\xi) = e^{-\beta V_i(\xi)} * \frac{\int e^{-\beta U_i(r)} \delta(\xi-\xi_i) dr}{\int e^{-\beta(U_i(r)+V_i(\xi))} dr} \quad (3.10)$$

Equation 3.10 can be rearranged to write it in terms of Equation 3.8 as shown in Equation 3.11.

$$P_i^u(\xi) = P_i^b(\xi) * e^{\beta V_i(\xi)} * \langle e^{-\beta V_i(\xi)} \rangle \quad (3.11)$$

Hence using Equation 3.6, we can easily obtain $A_i(\xi)$ as shown in Equation 3.12.

$$A_i(\xi) = -\frac{1}{\beta} \ln \left(P_i^b(\xi) \right) - V_i(\xi) + F_i \quad (3.12)$$

Where $F_i = -\frac{1}{\beta} \ln \left(\langle e^{-\beta V_i(\xi)} \rangle \right)$ is dependent on bias potential and is undetermined.

Free energy of each window can be readily obtained from the biased MD simulations. The only assumption made in the derivation is that the system is ergodic and the sampling in each window is sufficient. Now, the free energy curves of different windows are to be combined to obtain a global free energy curve $A(\xi)$. Therefore, it is required to calculate F_i . However, different simulations have different offsets (biases) and there is uncertainty in relation to how to weigh them. This is achieved using a special technique, the Weighted Histogram Analysis Method, discussed in the next section.

Bias potentials of any functional form can be chosen, but harmonic forms are generally employed because for their simplicity.

3.2.5 Weighted Histogram Analysis Method (WHAM)

The Weighted Histogram Analysis Method (WHAM) was developed by Kumar *et al.*, [52] and Ferrenberg and Swendsen [53], [54] to obtain the optimal estimate of an unbiased probability distribution from biased probability distributions generated using Umbrella sampling. In other words, WHAM provides a way to estimate F_i and stitch the information obtained from each sampling window together to yield a single unbiased probability distribution. The global distribution is obtained by a weighted average of the distribution of the individual windows. The weights (w_i) are chosen in order to minimize the statistical error of an unbiased probability distribution, P_u ($\sum w_i = 1$).

$$P^u(\xi) = \sum_i^{windows} w_i(\xi) P_i^u(\xi) \quad (3.13)$$

$$\frac{\partial \sigma^2(P^u)}{\partial w_i} = 0 \quad (3.14)$$

The WHAM equations for a one dimensional reaction coordinate are given by Equations 3.15 and 3.16.

$$P^u(\xi) = \frac{\sum_i^{windows} n_i P_i^b(\xi)}{\sum_j^{windows} n_j e^{-\beta(V_j(\xi) - F_j)}} \quad (3.15)$$

$$e^{-\beta F_i} = \int e^{-\beta V_i(\xi)} P^u(\xi) d\xi \quad (3.16)$$

Equation 3.15 and 3.16 are solved iteratively until convergence to obtain an unbiased probability distribution.

3.3 Metrics Used to Characterize the Simulation System

3.3.1 Radial Distribution Function (RDF)

The radial distribution function, $g(r)$, is defined as “the probability of finding a pair of atoms a distance, r , apart, relative to the probability expected for an ideal gas (random distribution) at the same density” [50]. This is a useful tool to describe the local structure of a system, for liquids in particular. In addition, certain thermodynamic properties like energy, pressure, chemical potential etc., can be calculated using $g(r)$. However, in this work $g(r)$ is used only to describe the local structure of a liquid.

Consider a liquid system containing N particles described using the LJ parameters, σ and ϵ . Also consider a spherical shell of thickness, δr , at a distance r from a desired particle. Let the bulk number density of the system be ρ . The, average number of particles present (N_{ideal}) in this volume element is given by Equation 3.17

$$N_{ideal} = \frac{4\pi\rho}{3} ((r + \delta r)^3 - r^3) \quad (3.17)$$

In order to find the local structure from MD simulations, the minimum image separations of all the relevant pairs of atoms are calculated and sorted into a histogram where each bin has width δr and extends from r to $r + \delta r$. This calculation is performed for all the configurations collected and is normalized. Then parameter $g(r)$ is given by Equation 3.18 where N_{actual} represents the average number of particles present in the bin, spanning from r to $r + \delta r$

$$g(r) = \frac{N_{actual}}{N_{ideal}} \quad (3.18)$$

Liquids do not possess long-range structure; hence beyond a certain distance, $g(r)$ of the liquid system will be 1 implying a random structure. Short-range order is reflected by peaks and troughs in the $g(r)$. A typical radial distribution function of liquid water (SPC/E model) calculated from MD simulation is shown in Figure 8. Note $g(r)$ is zero at short distances because of the strong repulsive forces arising from the Lennard-Jones system of atoms (atoms have an excluded volume and cannot penetrate into one another). The peaks represent the solvation shells, note that after 8\AA , there is no structure.

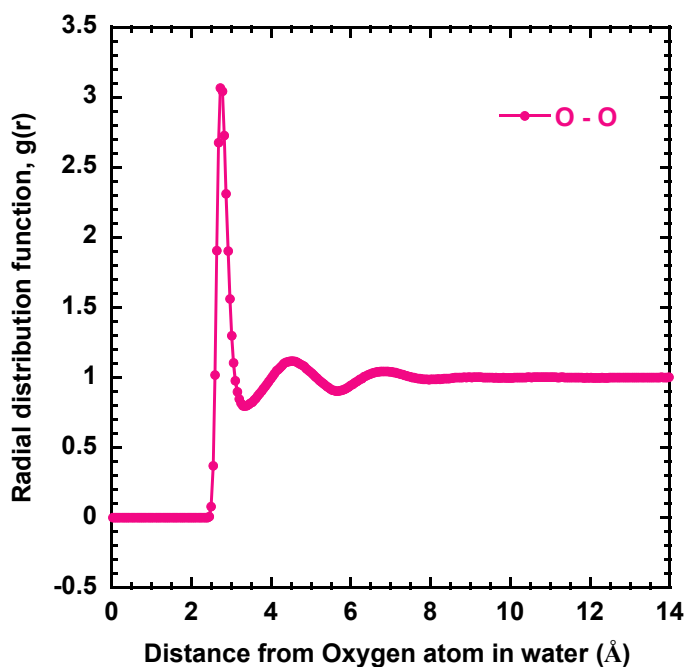


Figure 8: Radial distribution function of SPC/E water.

3.3.2 Diffusion Coefficient Using Mean Squared Displacement

In molecular simulations, transport coefficients may be calculated using equilibrium velocity correlation functions or by the Einstein relation. The Einstein relation

is adopted in this work. The motion of a particle in a liquid is considered as a good approximation of a stochastic random walk process. As they move, the particles in the fluid collide with other particles resulting in non-directed movements. These movements are characterized by relating mean squared displacement and the lag time [55]. The relationship for a three dimensional system is given by Equation 3.19.

$$\langle |\mathbf{r}_i(t) - \mathbf{r}_i(0)|^2 \rangle = 6Dt \quad (3.19)$$

Where D is the diffusion coefficient, t is the time elapsed and $\mathbf{r}_i(t)$ is the position of the particle. The left of Equation 3.4 gives the mean squared displacement (msd) and is calculated from the MD simulation. The slope of msd vs. time gives the diffusion coefficient.

Statistical accuracy is improved by measuring the mean squared displacement of all the desired particles in the simulation system, the results are added together and divided by the number of particles. For molecules, the msd of the center of mass is computed and, as Equation 3.19 is valid only at long times, simulations should be run long enough so a perfect straight line for msd vs. time is observed.

3.3.3 Gyration Tensor

The gyration tensor (S) is used to describe the distribution of particles that are clustered together [56]. For a system of N particles, the gyration tensor is defined as follows.

$$S_{ij} = \frac{\sum_{k=1}^N m_k (r_i^k - r_i^{CM})(r_j^k - r_j^{CM})}{\sum_{k=1}^N m_k}; S = \begin{pmatrix} S_{xx} & S_{xy} & S_{xz} \\ S_{yx} & S_{yy} & S_{yz} \\ S_{zx} & S_{zy} & S_{zz} \end{pmatrix} \quad (3.20)$$

Where CM represents the center of mass of the N particles and m_k is the mass of the k^{th} particle.

Size and shape factors of the cluster are calculated from the principal moments (Eigen values) that describe the distribution of particles. If λ_1, λ_2 and λ_3 represent the principal moments ($\lambda_1 > \lambda_2 > \lambda_3$), then the size of the cluster is defined by a radius of gyration (Equation 3.21) and shape factors, asphericity and acylindricity, are defined by Equation 3.22 and 3.23, respectively.

$$R_g^2 = \lambda_1 + \lambda_2 + \lambda_3 \quad (3.21)$$

$$b = \frac{\lambda_1 - \frac{1}{2}(\lambda_2 + \lambda_3)}{R_g^2} \quad (3.22)$$

$$c = \frac{\lambda_2 - \lambda_3}{R_g^2} \quad (3.23)$$

The radius of gyration shows the mass distribution of atoms with respect to the center of mass of the cluster. This gives a good representation of size of the cluster. As seen in Equation 3.21, the asphericity is always non-negative and is zero when the distribution of particles is spherically symmetric. Similarly, acylindricity is always non-negative and is zero when the distribution of particles is cylindrically symmetric.

3.4 Simulation System to Study Aggregation Behavior in Bulk Aqueous Phase

Since the objective is to study the effect of chemistry, the simulation system is represented in full atomistic detail. Imidazoline derivatives are chosen as model corrosion inhibitors as they are proven to be effective in inhibiting corrosion and, hence, they are a good choice to understand underlying fundamental mechanisms. The selected inhibitor molecules are designed using advanced molecular editing software ‘Avogadro’.

As discussed in chapter 2, these inhibitors are likely to accept a proton when present in an aqueous phase as it would result in a conjugated system that has a lower energy (Figure 9). The imidazoline ring has two nitrogens and any one of them could accept a proton, however, steric hindrance makes it difficult for a proton to approach the nitrogen that has the pendent group attached. This was confirmed by calculating the single point energy (SPE) for both the configurations using GAUSSIAN-09 software. A typical structure of the molecule that is used for simulations is shown in Figure 10.

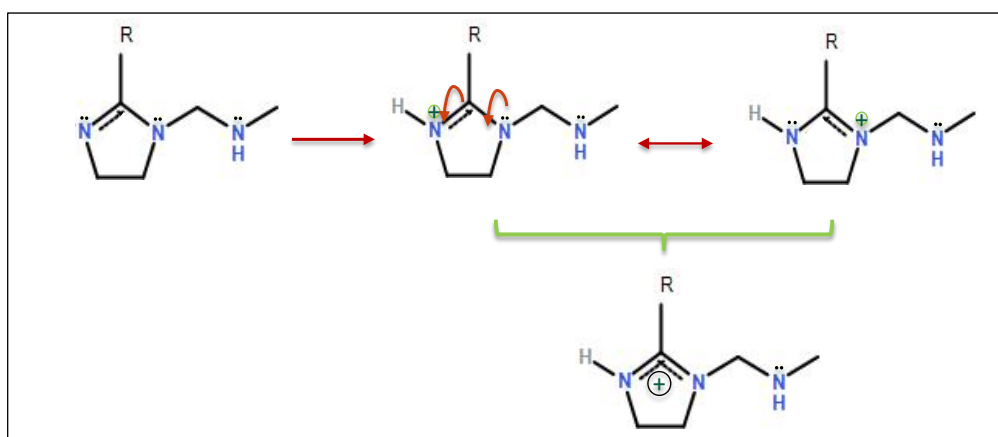


Figure 9: Schematic showing electron delocalization on the imidazoline ring on accepting a proton.

Protonation is critical because it creates a net positive charge on the inhibitor molecule, and the protonation site affects the partial charge distribution on the adjacent atoms that is expected to influence inhibitor interactions. Structures of inhibitor molecule were optimized and atomic partial charges calculated in the presence of implicit water (as solvent) using density functional theory (DFT) with GAUSSIAN-09. DFT theory level of B3LYP and 6-31G (d, p) orbital basis sets were used in geometry optimization calculations.

During molecular dynamics runs, the inhibitor molecules may take different conformations due to the presence of hydrophobic tails and explicit water, but the partial charges are not recalculated in each time step. Also there is no breaking / making of chemical bonds in a MD run; care must be taken in choosing the structure and parameters of initial model inhibitor molecules.

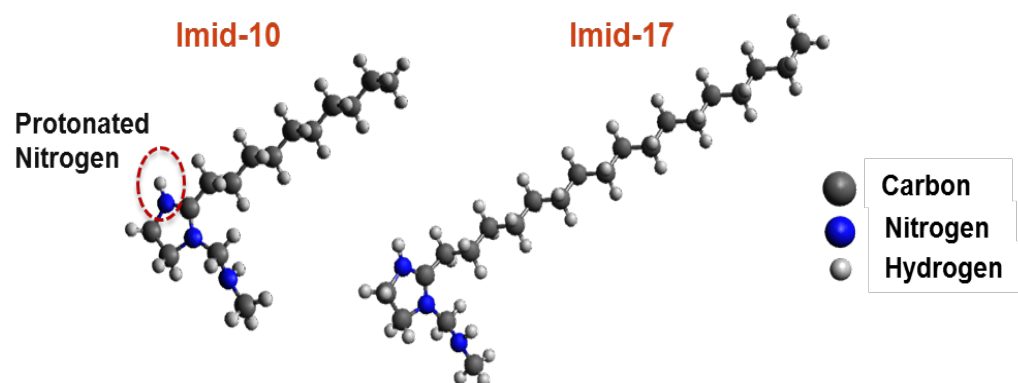


Figure 10: Structure of the two imidazolinium derivative molecules (Imid-10 & Imid-17) that are employed in the simulations.

The charge distribution is generally affected by the presence of hetero-atoms. A homologous series of compounds should not be very different w.r.t the partial charges on their head group. This was confirmed by measuring partial charges for molecules with different alkyl tail lengths where **N** corresponds to the number of carbon atoms therein (see Tables 1 & 2).

Table 1: Partial charges with hydrogens summed into heavier atoms for imidazolium ring and pendant group; atom positions labelled in Figure 11.

Atom	N = 4	N = 5	N = 6	N = 9	N = 11	N = 17
C1	0.231425	0.339979	0.443651	0.297665	0.238325	0.287082
N1	0.039656	-0.028200	-0.001871	0.010966	0.029786	0.027148
N2	-0.128311	-0.083092	-0.179890	-0.157047	-0.181747	-0.132366
C2	0.155813	0.206879	0.183443	0.180770	0.222004	0.230080
C3	0.249884	0.192297	0.218114	0.228844	0.182077	0.159831
C4	0.306896	0.270421	0.257175	0.315622	0.332956	0.315917
N3	-0.179398	-0.211029	-0.145724	-0.158274	-0.205701	-0.167142
C5	0.150766	0.177935	0.143274	0.140176	0.165216	0.153918

Table 2: Average of partial charges from Table 1.

Atom	Avg. charge	Std. dev
C1	0.306355	0.078320
N1	0.012914	0.024961
N2	-0.143742	0.037347
C2	0.196498	0.028139
C3	0.205175	0.033112
C4	0.299831	0.029461
N3	-0.177878	0.026111
C5	0.155214	0.014188

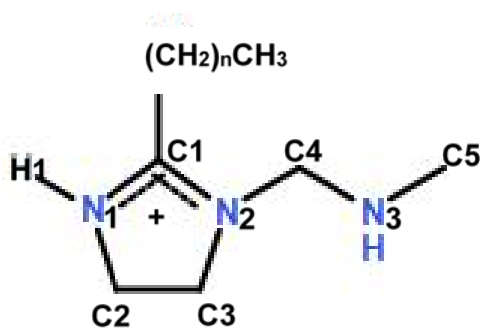


Figure 11: Imidazolium ring along with the pendant group. C1, C2, C3, C4, C5, N1, N2, N3 & H1 are only references to particular position.

The MD simulation system consists of imidazolinium-type corrosion inhibitors, immersed in liquid water at $T = 300\text{ K}$ and $P = 1\text{ bar}$. To maintain charge neutrality in the system, equal amounts of chloride ions are placed in the simulation box (Figure 12). All atoms are simulated as simple Lennard-Jones (LJ) atoms with characteristic σ & ϵ . The inhibitor interactions are simulated using the General Amber Force Field (GAFF) [57] that has a functional form shown in Equation 3.4. Chlorides are represented using the Joung-Cheatham model [58] and the simple point charge model (SPC/E) [59] was adopted to simulate water. Interatomic interactions were modeled as a combination of Lennard-Jones (LJ) and Coulombic potentials. The particle-particle-particle mesh (PPPM) Ewald method [50] was used to account for long-range Coulombic interactions. In SPC/E model, water is represented as 3-site rigid molecule with constant angle (109.4°) and constant bond length (1 \AA); this was achieved using SHAKE algorithm. Periodic boundary conditions are applied on all faces of the simulation box and a spherical cut-off of 9.8 \AA is chosen for LJ interactions, with a 14 \AA cutoff for Coulombic interactions.

Since the key research focus is establishing the aggregation and diffusion behavior of molecules with different degrees of hydrophobicity, two imidazolinium molecules, one with an alkyl tail consisting of 10 saturated carbons ($-(\text{CH}_2)_9\text{CH}_3$) and another with 17 saturated carbons ($-(\text{CH}_2)_{16}\text{CH}_3$), are studied (see Figure 10). These inhibitor molecules are referred to as Imid-10 & Imid-17 throughout the document. Two sets of simulations were conducted with different objectives. In the first set of diffusion simulations the effect of inhibitor concentration on diffusion was explored, an initial cubic box length of 50 \AA was chosen and concentration of inhibitor molecules was varied by keeping the size of the

simulation box constant and increasing the number of inhibitor molecules; concentrations sampled range from 0.02 M – 0.9 M. In the second set of diffusion simulations, effect of cluster size (by cluster size, this refers to the number of inhibitor molecules that are aggregated to form a cluster) on diffusion was explored by conducting all simulations at the same inhibitor concentration of 0.09 M. The number of inhibitor molecules sampled range from 2 to 36. More details on this are given in section 4.2. The time step was 1 femtosecond. Using Nose-Hover thermostat and barostat [60], [61], MD simulation of the NPT ensemble was conducted for 15 nanoseconds, where the initial 3 – 6 nanoseconds was the equilibration time. All MD simulations were performed using the Large-Scale Atomic/Molecular Massively Parallel Simulation (LAMMPS) package [62].

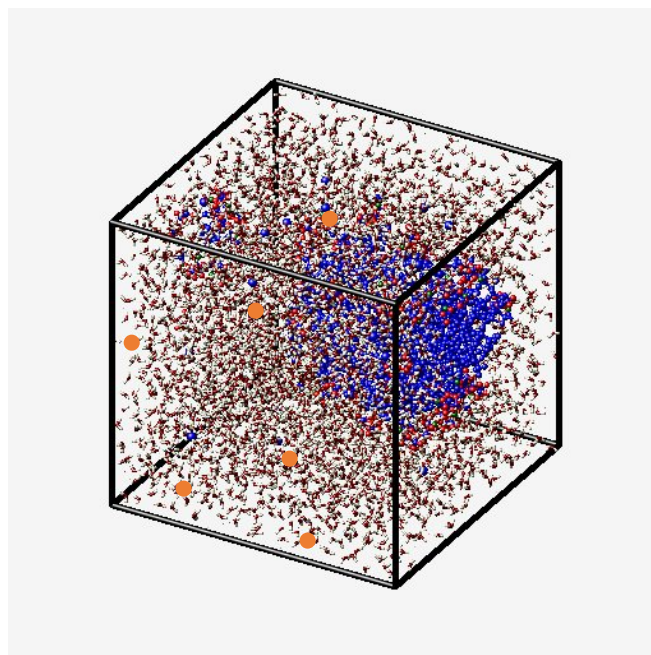


Figure 12: Snapshot of a typical MD simulation that is used for studying aggregation and diffusion properties; blue represents alkyl tail, red represents hydrophilic head, orange represents chlorides and maroon represents water molecules.

3.5 Simulation System to Generate Free Energy Landscapes of Adsorption

The simulation system used is similar to the one described in the previous section. Additionally, a metal surface (Au) is introduced in the z-direction that would create a metal-water interface. The metal atoms are simulated as neutral LJ atoms ($\sigma = 2.629\text{\AA}$ and $\varepsilon = 5.29 \text{ KCal/mole}$) according to the model developed by Heinz, *et al.* [63], [64]. A gold surface is simulated as it is typically used in experimental research on adsorption of amphiphilic molecules, such as corrosion inhibitors, because of its inert nature. Six layers of metal atoms are placed in a close packed face-centered cubic (*fcc*) lattice plane (111) with lattice constant of 4.08\AA . Periodic boundary conditions are imposed in x & y direction while the z-direction is non-periodic. The length of the box along the z-direction is maintained sufficiently long (~ 3 times the length of x or y direction) to avoid self-interaction of metal atoms. About 5\AA of vapor space is maintained at the top of the aqueous phase along the z-direction which will maintain the system at equilibrium pressure corresponding to $T = 300\text{K}$. All simulations involving the metal are carried out using a canonical ensemble (constant N, V and T). Introduction of a metal surface is expected to affect the density of water molecules locally at the interface as they are exposed to a different environment. MD simulation of an NVT ensemble of water in the presence of the Au metal surface resulted in layering of water at the metal-water interface, Figure 13. The density profile was generated by slicing the simulation system into different cuboids of width 0.5\AA along the z-direction. Two distinct peaks were observed at 2.4\AA and 5.5\AA from the metal surface which correspond to $\frac{\sigma_{metal} + \sigma_{oxygen}}{2}$ & $\frac{\sigma_{metal} + \sigma_{oxygen} + \sigma_{oxygen}}{2}$, respectively. The peaks indicate the ordered orientation of water molecules, *i.e.*, two layers

of water molecules are strongly adsorbed to the metal surface. The spherical cut-off for LJ interactions for the metal is set at 12\AA and those water molecules beyond this cut-off are uninfluenced by the metal surface and, hence, maintain the density of 1 g/cc .

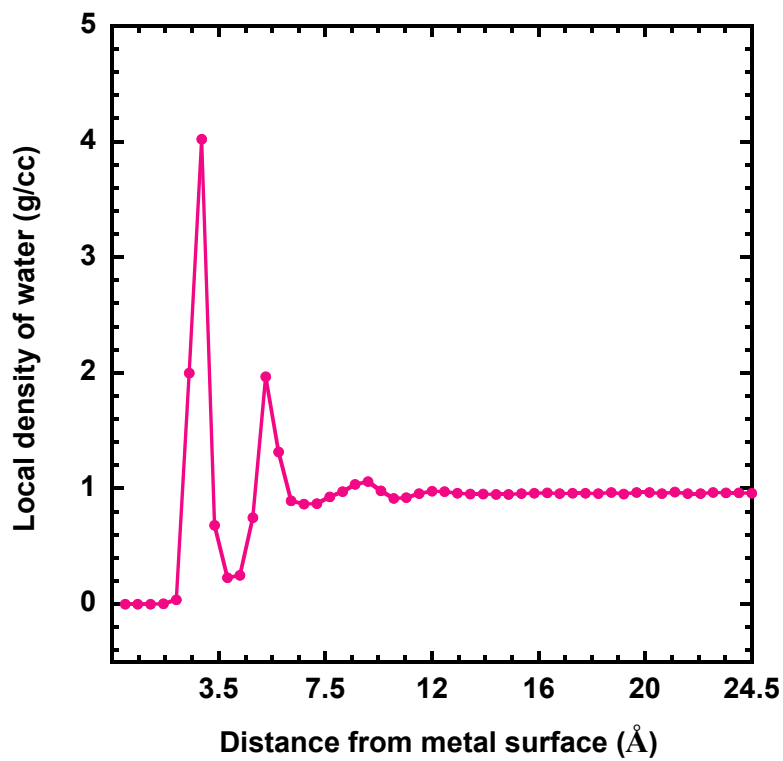


Figure 13: Density profile of water in the presence of a metal surface as a function of distance from the metal surface.

Six layers of metal atoms are considered in the simulation as the water density profile is unaffected with further increase in metal atomic layers, also the top three layers of metal are considered mobile while the bottom three layers are kept rigid. This methodology is followed to save computational time. A typical adsorption simulation system is shown in Figure 14.

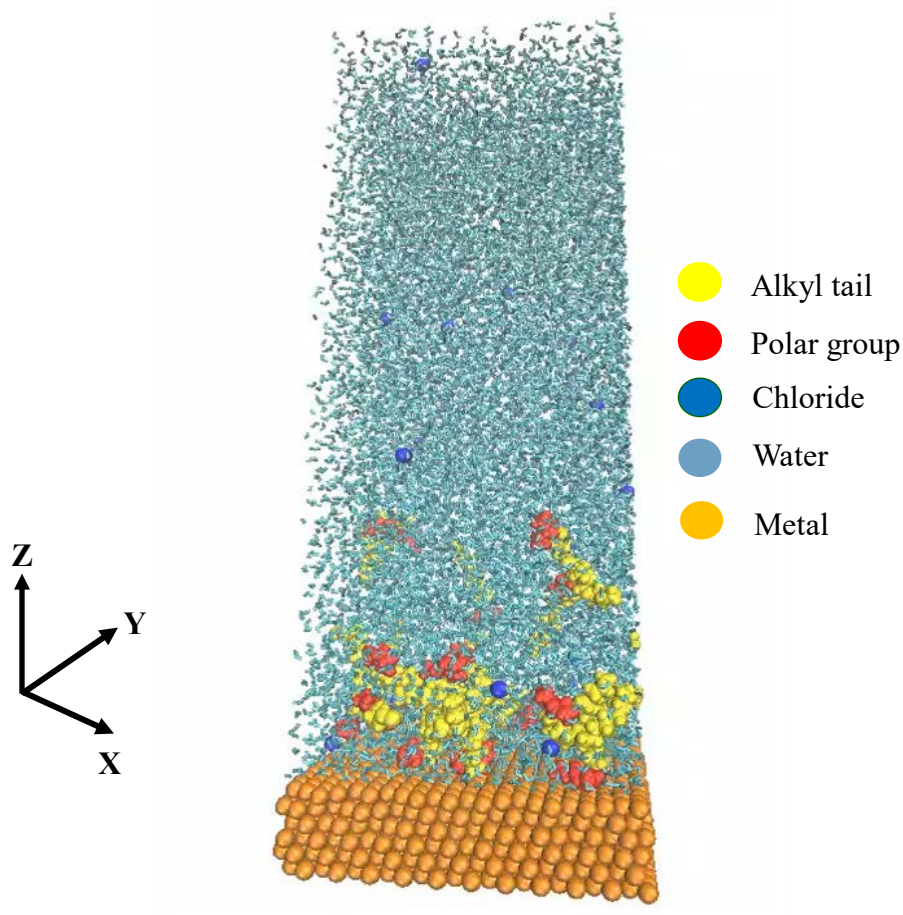


Figure 14: Snapshot of a MD simulation system that is used to study adsorption.

Initially, efforts were made to study the formation of self-assembled monolayer at different concentrations of Imid-17 & Imid-10. However, it was observed that the inhibitor molecules aggregate rapidly in the bulk aqueous phase and are limited by diffusion barriers from reaching the metal surface. The interaction of inhibitors with the adsorbed water layers and metal was unclear from these sets of simulations. For an inhibitor molecule to adsorb on the metal surface, the water layers on the metal surface are to be displaced. Hence the adsorption process was expected to involve a free-energy barrier. Therefore, it was

desirable to obtain the free energy landscape for the adsorption of an inhibitor molecule at infinite dilution (where there is no interaction with other inhibitor molecules) and that of a cluster (strong inhibitor-inhibitor interactions exist within the cluster). Free energy landscapes of adsorption are calculated along the z-axis using Umbrella sampling.

4 RESULTS & DISCUSSION

4.1 Diffusion as a Function of Concentration and Hydrophobicity

Figure 15 show the diffusion coefficient of inhibitor molecules calculated from MD simulations conducted at different inhibitor concentration. The concentration is varied by keeping the size of the simulation box constant at 50\AA and increasing the number of inhibitor molecules. The trajectories were collected for about 15 nanoseconds with the first 3-6 nanoseconds being equilibration time. Diffusion coefficient was measured from the slope of mean-squared displacement vs. time data (see section 3.3.2). With increase in concentration, the diffusion coefficient decreases for both Imid-10 & Imid-17, as would be expected.

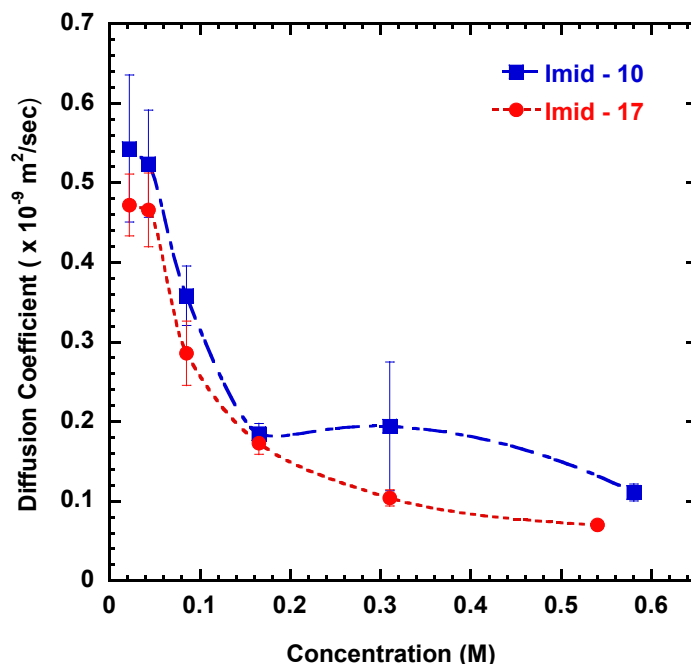


Figure 15: Diffusion coefficient of imidazolium-type corrosion inhibitors as a function of concentration and hydrophobicity (tail length).

The large error bars in the case of Imid-10 are because of the presence of different sized clusters as the system evolves with time, *i.e.*, hydrophobic alkyl tails in inhibitor molecules tend to avoid interaction with water by interacting with each other. This results in formation of clusters and effective diffusion of the inhibitors decreases due to increased size. Imid-17 being more hydrophobic, molecules aggregate rapidly (~ 1 nanosecond) while Imid-10 molecules take a longer time for this phenomenon to take place, – hence a direct comparison between Imid-10 & Imid-17 cannot be made. The decrease in diffusion coefficient seen in these simulations is a consequence of both the concentration and aggregation effects. However, care has to be taken interpreting such data as trends would change, if the trajectories are collected for a longer time. At higher concentrations, in the case of Imid-17, it was observed that all the inhibitors in the simulation box aggregate together to form a cluster that has a diameter larger than half the box length. This causes finite size effects such as formation of system-spanning micelles (Figure 16) and interaction with periodic images.

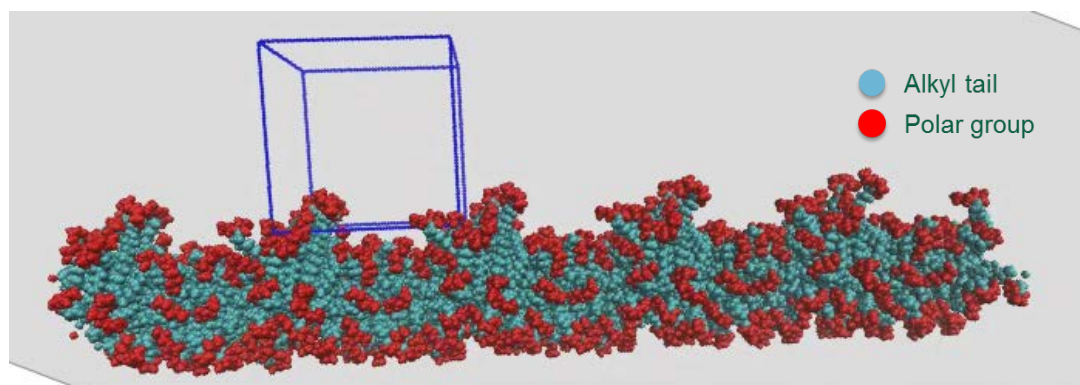


Figure 16: System spanning cylindrical micelle formed by Imid-17 inhibitors at 0.9M concentration. Water molecules and chlorides are not shown in this snapshot. Periodic images of cluster are shown along the x-axis to visualize the infinite micelle.

Finite size effects can be avoided by using a bigger simulation box, but this will increase the computational time. Also, the system evolves much slower because of diffusion barriers. In order to overcome this problem, a new set of MD simulations were conducted using a different methodology. It shall be noted that all the concentrations sampled here are much larger than a typical CMC of 30 to 40 mM. At concentrations above CMC, it is likely that a distribution of clusters with different aggregation numbers will be observed.

4.2 Diffusion as a Function of Cluster Size and Hydrophobicity

This set of MD simulations were all conducted at the same inhibitor concentration of 0.09M using an NPT ensemble at $T = 300\text{K}$ and $P = 1\text{ bar}$. 500 water molecules per inhibitor are considered, hence, the size of the simulation box is different for each simulation. The idea here is to evolve the system long enough to initially form a ‘single cluster’ that has all the inhibitor molecules in the simulation box aggregated together. When greater number of inhibitor molecules are present in the system, the aggregation process may be slow; particularly true in the case of Imid-10. Here, the aim is to obtain an unbiased equilibrium cluster structure – The aggregation process was accelerated by removing one-third of the water molecules (randomly picked) after the system had aggregated into three or four separate clusters. Once the single cluster was formed, the removed water molecules are added back and trajectories are collected for about 15ns. The data is collected for analysis after ensuring that the single cluster that was formed is in equilibrium, *i.e.*, the structure of the cluster is not changing significantly. One can think of this as diffusion of different sized clusters at infinite dilution. Here-on, cluster size

corresponds to the ‘number of inhibitor molecules present in the cluster’ unless stated otherwise. Figure 17 show the diffusion data obtained for different cluster sizes. Imid-17 molecules diffuse slower than Imid-10 molecules at all cluster sizes; the reason for this behavior is discussed in further sections. With increase in cluster size, diffusivity decreases. As more inhibitors aggregate together the size of the cluster is expected to increase, which decreases the diffusivity. However, the decrease is sharp until cluster size of 10 and then it decreases gradually. In order to validate the diffusion data, it is required to measure the diameter of clusters. This was done by determining the mean squared radius of gyration of the cluster.

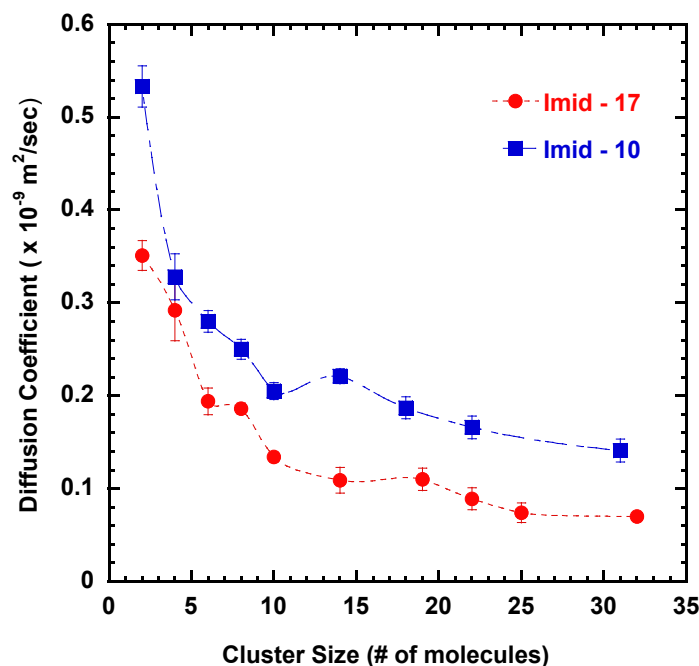


Figure 17: Effect of cluster size/aggregation number and hydrophobicity on diffusion coefficient of imidazolinium-type corrosion inhibitors.

Radius of gyration (R_g) for different sized clusters is shown in Figure 18. With increase in aggregation number, R_g of the cluster increases. This is expected because more inhibitor molecules need to be accommodated which increases the volume. Another stark observation is that R_g of Imid-17 & Imid-10 clusters are almost equal when aggregation number is more than 8 molecules. This is counter-intuitive because R_g of a single Imid-10 molecule is *ca.* 4.5Å while Imid-17 is *ca.* 7Å. This implies that the shape of the clusters and orientation of molecules therein is different for Imid-10 & Imid-17. Since R_g is an average measure of all three Eigen values, it does not reveal any information on either the shape or orientation of the molecules in the clusters.

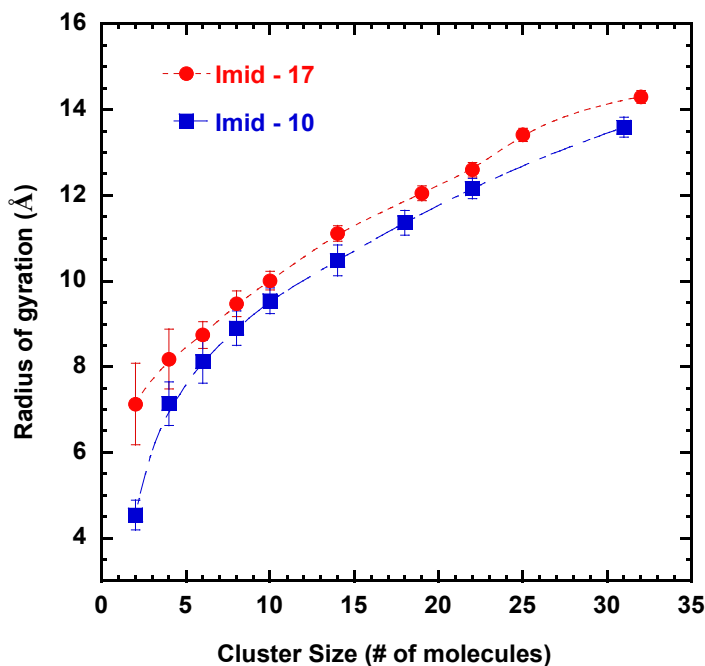


Figure 18: Effect of hydrophobicity on root mean squared radius of gyration (R_g) of clusters with different aggregation numbers.

In order to find the shape of clusters, shape factors elucidated in section 3.3.3 are calculated using Eigen values of gyration tensor. The trend in asphericity and acylindricity values are shown in Figure 19. It is very clear from the graphs that both acylindricity and asphericity values go to zero as aggregation number increases for either Imid-17 or Imid-10. This suggests that the periphery of the clusters does look like a spherical cluster. Also, examination of Eigen values (Figure 20) suggest that imid-10 and imid-17 clusters have the same size in all three dimensions. Trends observed for all Eigen values suggest that clusters are growing in all three dimensions.

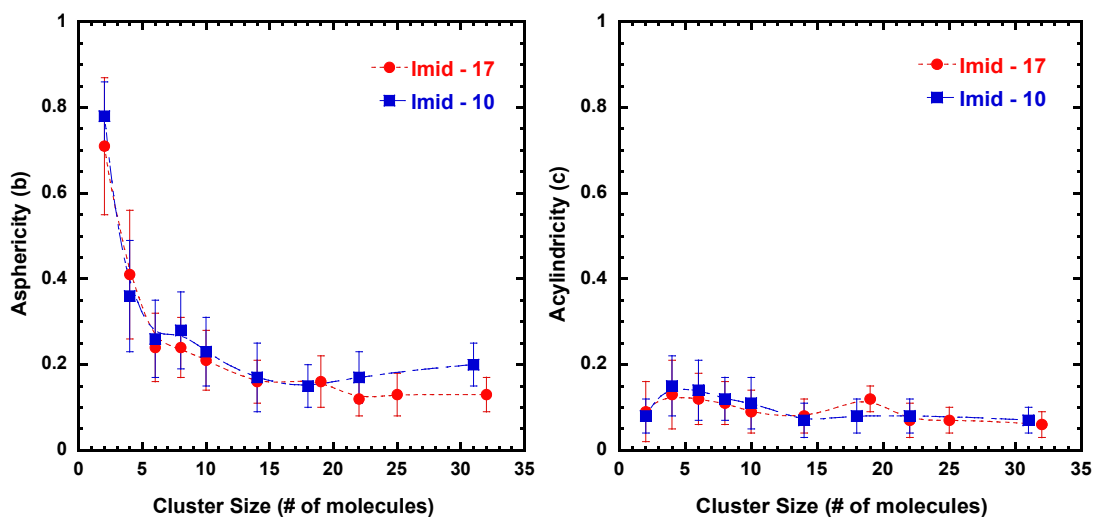


Figure 19: Shape factors calculated using Eigen values of gyration tensors for different clusters; asphericity and acylindricity are shown as a function of cluster aggregation number and hydrophobicity.

The shape factors suggest that both Imid-10 and Imid-17 form increasingly spherical clusters with increase in aggregation number. Therefore, assuming the cluster to

be a spherical particle with radius equivalent to its R_g , the diffusion coefficient was estimated theoretically using the Stokes-Einstein relation (Equation 4.1).

$$D = \frac{kT}{6\pi a\eta} \propto \frac{1}{a} \quad (4.1)$$

Where ' k ' is the Boltzmann's constant, ' T ' represent temperature

' η ' is the viscosity of solvent medium (water in this case) and

' a ' corresponds to hydrodynamic radius of the spherical particle

At $T = 300\text{K}$ & $\eta = 0.0009 \text{ Pa}\cdot\text{s}$, and approximating ' a ' to ' R_g '. Then,

$$D = \frac{kT}{6\pi a\eta} \propto \frac{1}{a} \cong \frac{2.44 * 10^{-9}}{R_g} m^2 s^{-1} \quad (4.2)$$

Figure 21 & Figure 22 compare diffusion coefficient calculated from Equation 4.2 with the values obtained from MD simulations for Imid-10 & Imid-17 respectively. Theoretical values match well with the simulation values for Imid-10 clusters, providing strong evidence that the clusters formed by Imid-10 molecules are spherical in shape. However, simulation data for Imid-17 does not correlate with the Stokes-Einstein relationship. At aggregation number > 10 , the Stokes-Einstein relation over predicts the diffusion value by a factor of two.

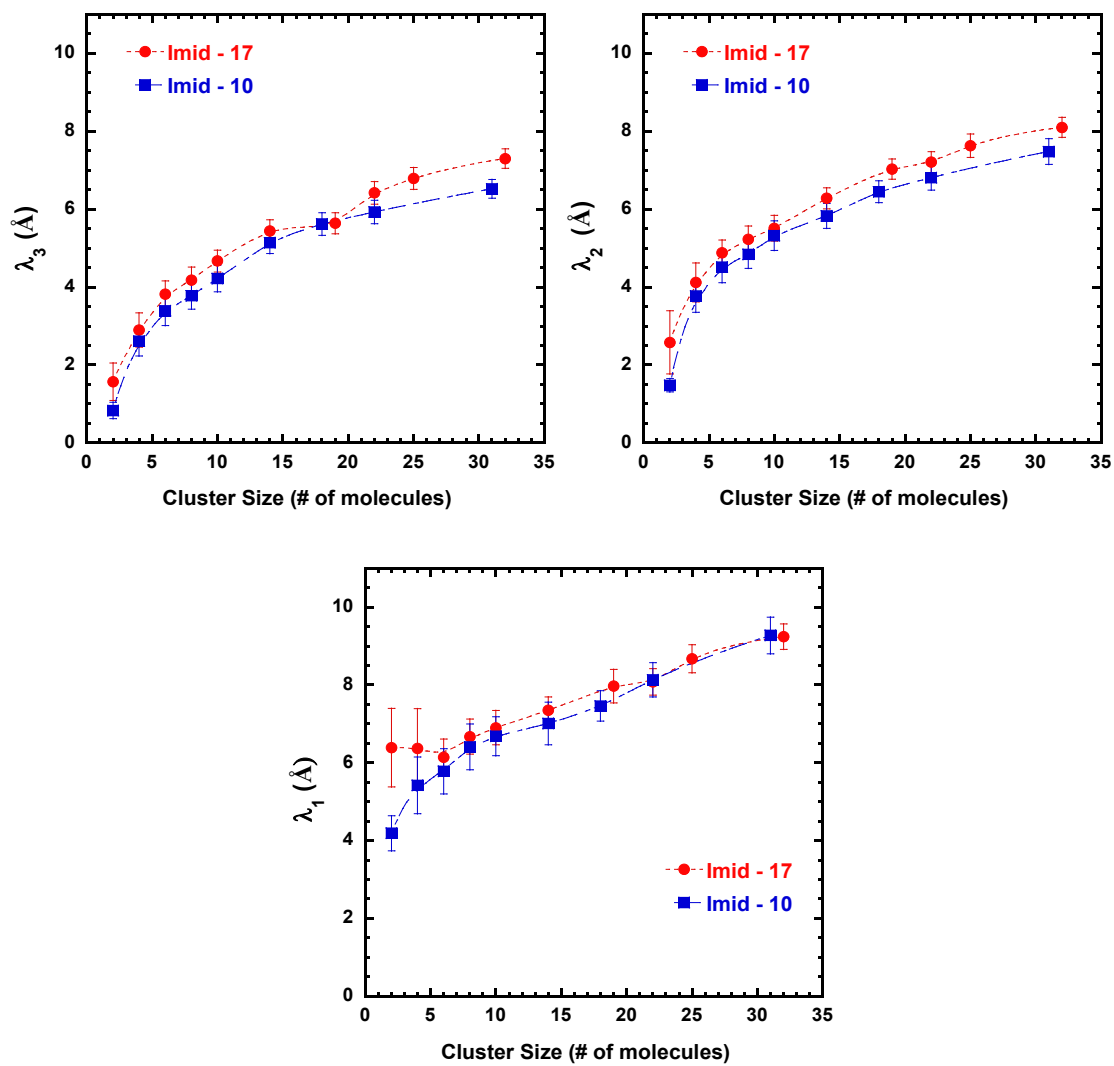


Figure 20: Eigen values of gyration tensors for different clusters.

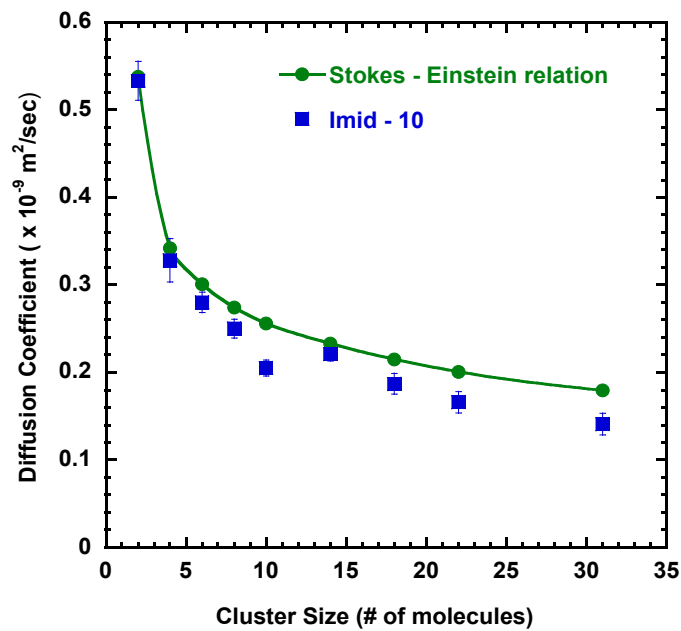


Figure 21: Diffusion coefficients of Imid-10 clusters calculated from the Stokes – Einstein relationship.

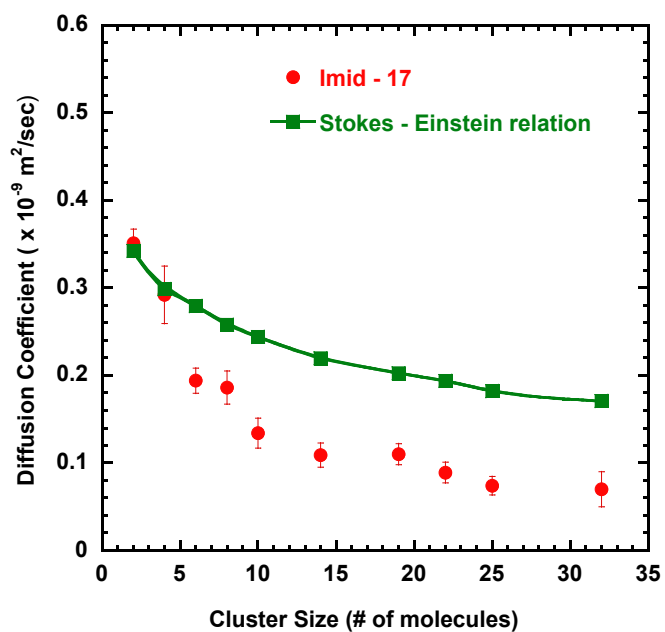


Figure 22: Diffusion coefficients of Imid-17 clusters calculated from the Stokes – Einstein relationship.

Shape factor analysis does not explain the diffusion data for Imid-17. In addition to shape, the other factor that can affect diffusion is orientation of molecules. Visualization of different clusters formed in MD simulations seem to suggest that Imid-10 & Imid-17 clusters pack differently and orientation of molecules is also different. Snapshots of different clusters are shown in Figures 23 & 24.

Visualizations show that all the polar groups (red color) are on the periphery while alkyl tails (cyan color) hide from water; the radial distribution of hydrophobic and hydrophilic atoms w.r.t center of mass of cluster confirms this (Figure 25). However, it appears that the molecules span through the diameter of the cluster, *i.e.*, instead of alkyl tails huddling in the center, the molecules stack over one another so that tails interact with each other and polar groups interact with water. This type of packing is energetically favorable when inhibitor molecules available are less than the critical micelle aggregation number.

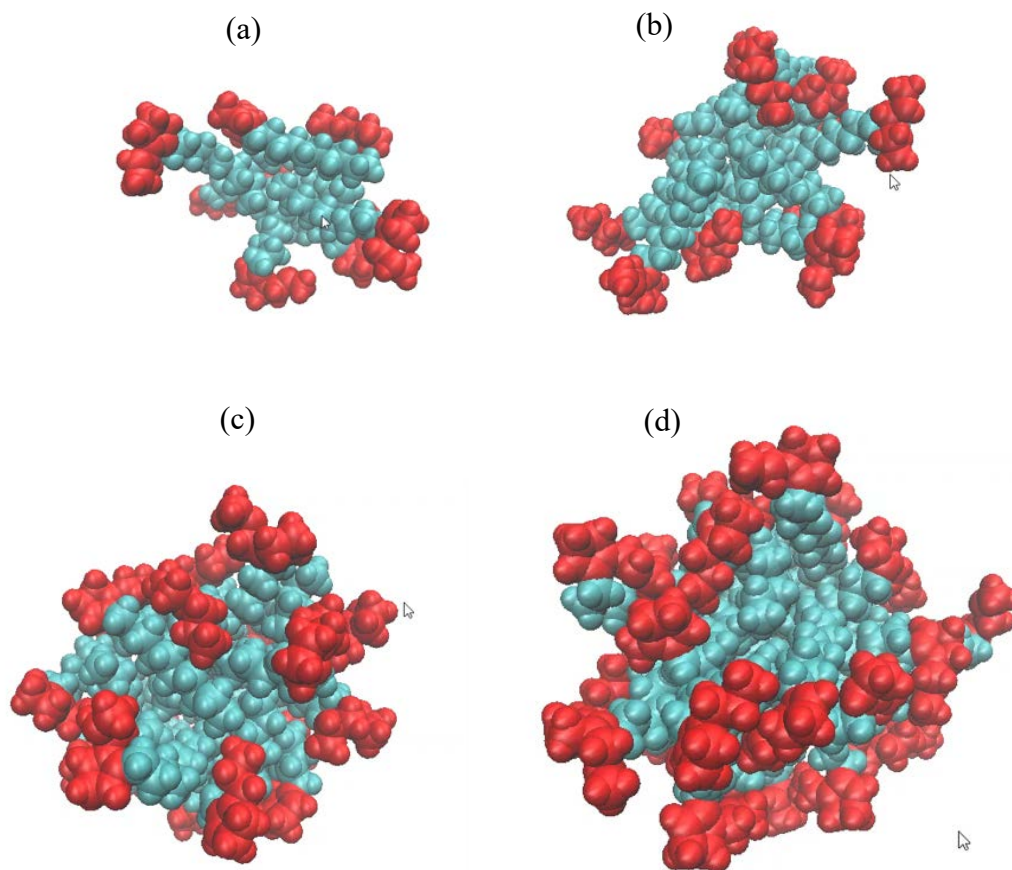


Figure 23: Snapshot of different sized clusters formed by Imid-10 molecules; red indicates hydrophilic head and cyan indicates alkyl tail: (a) 8 molecules; (b) 14 molecules; (c) 22 molecules; (d) 32 molecules.

The radial distribution of hydrophilic atoms (imidazolinium head group and pendant group) w.r.t center of mass of cluster show that the distance between center of mass of cluster and polar group increases as aggregation number increases (Figure 26). In other words, the head groups move away from the center of mass to accommodate more inhibitors and increase the inhibitor-inhibitor interactions. This keeps occurring until critical micelle aggregation number is reached and a perfect spherical micelle with no alkyl

interactions with water is formed. Further evidence of this mechanism is shown in Figure 27.

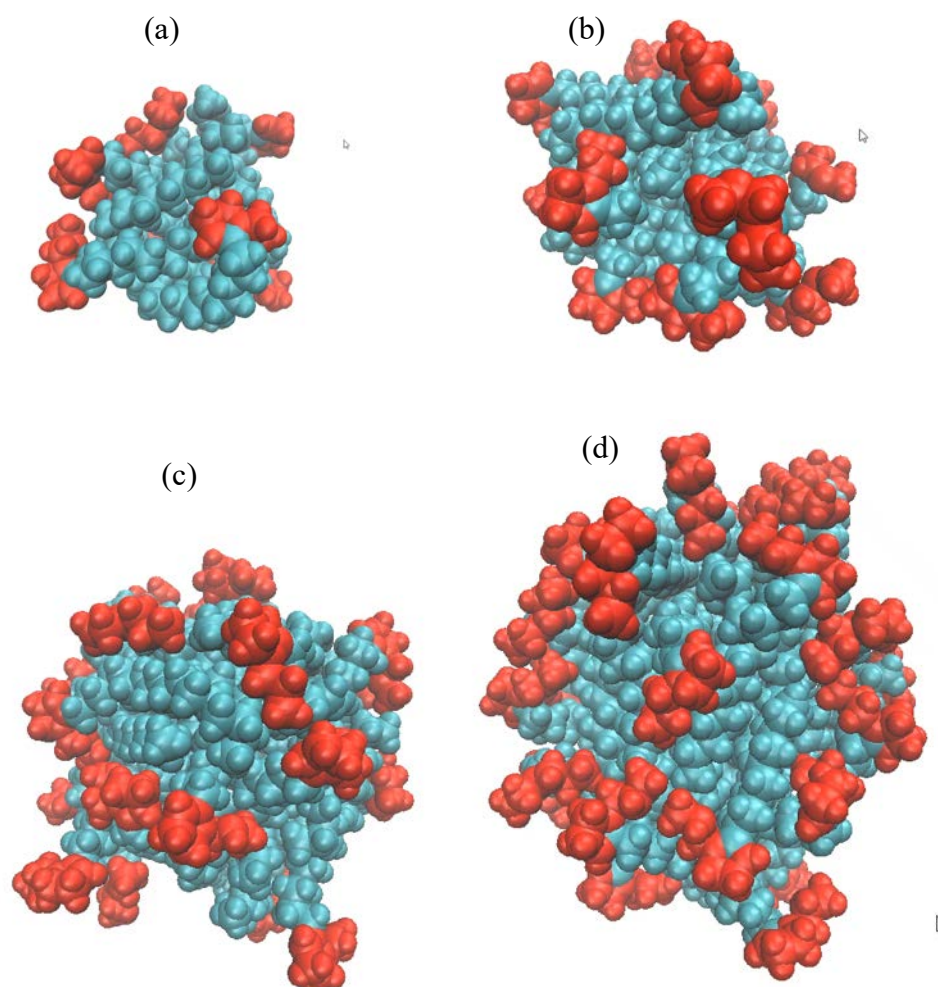


Figure 24: Snapshot of different sized clusters formed by Imid-17 molecules; red indicates hydrophilic head and cyan indicates alkyl tail: (a) 8 molecules; (b) 14 molecules; (c) 25 molecules; (d) 32 molecules.

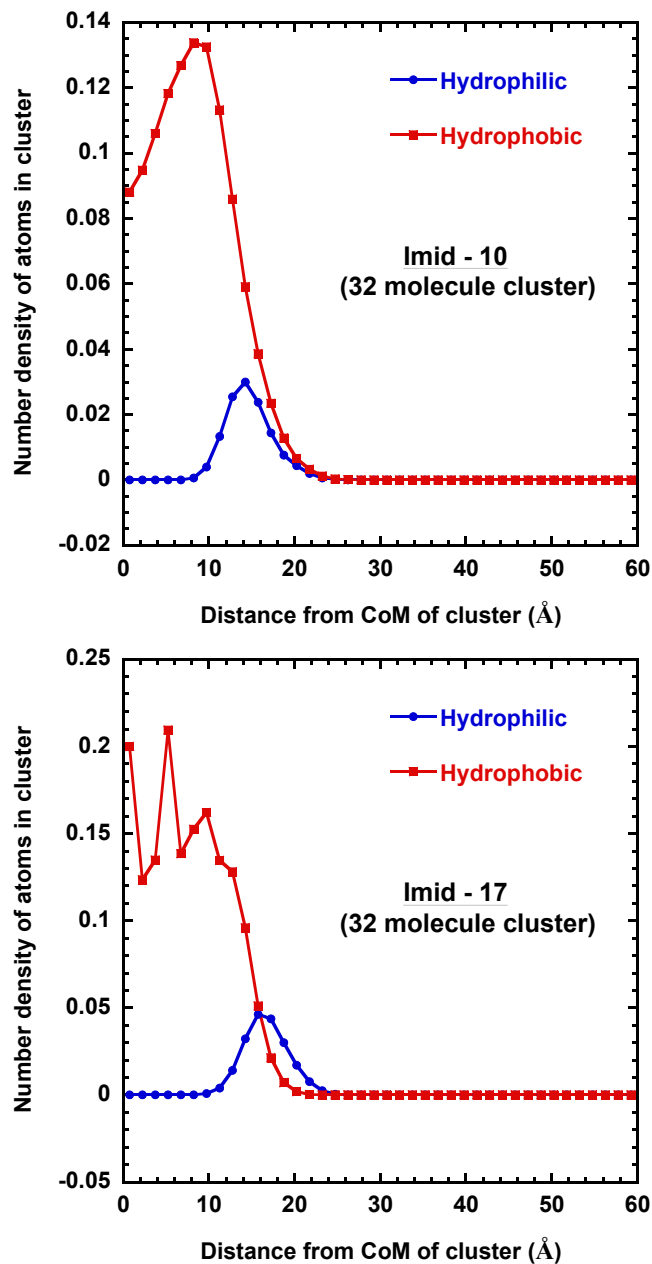


Figure 25: Radial distribution of atoms in a cluster w.r.t center of mass of cluster. 'Hydrophilic' refers to atoms on the imidazolinium ring & pendant group; 'Hydrophobic' refers to carbons in the alkyl tail.

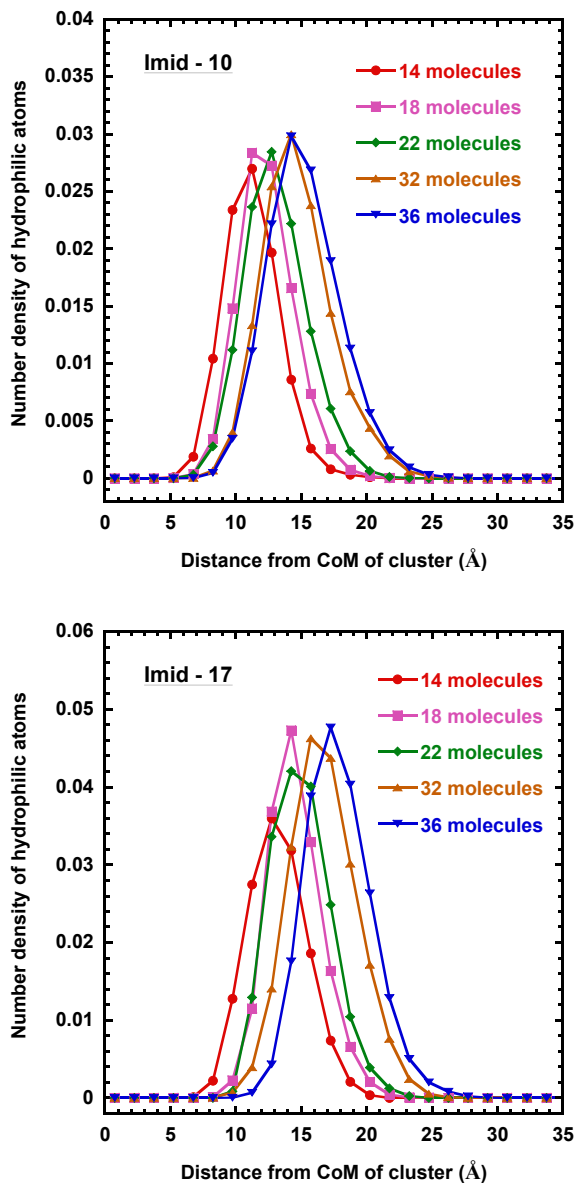


Figure 26: Radial distribution of hydrophilic atoms (atoms on the imidazolinium ring & pendant group) w.r.t. center of cluster.

Figure 27 show the radial distribution function, $g(r)$, of water around the terminal carbon on the alkyl tail. It is evident from the *rdf* that the terminal carbon of the alkyl tail is trying to hide from water and, with increase in aggregation number, it further moves

inside and hides more effectively (observe the decrease in $g(r)$ with increase in cluster size). RDF becomes 1 at about two times R_g , this confirms that the molecules span throughout the diameter of the cluster. A schematic of this mechanism is shown in Figure 28.

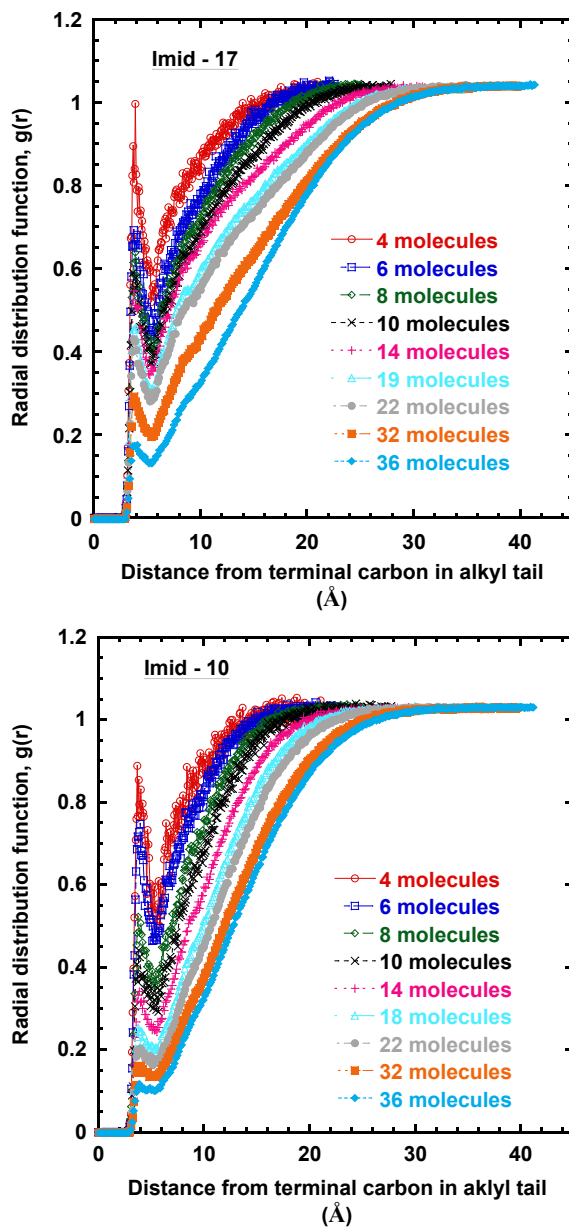


Figure 27: Radial distribution function of water w.r.t. terminal carbon as a function of cluster size.

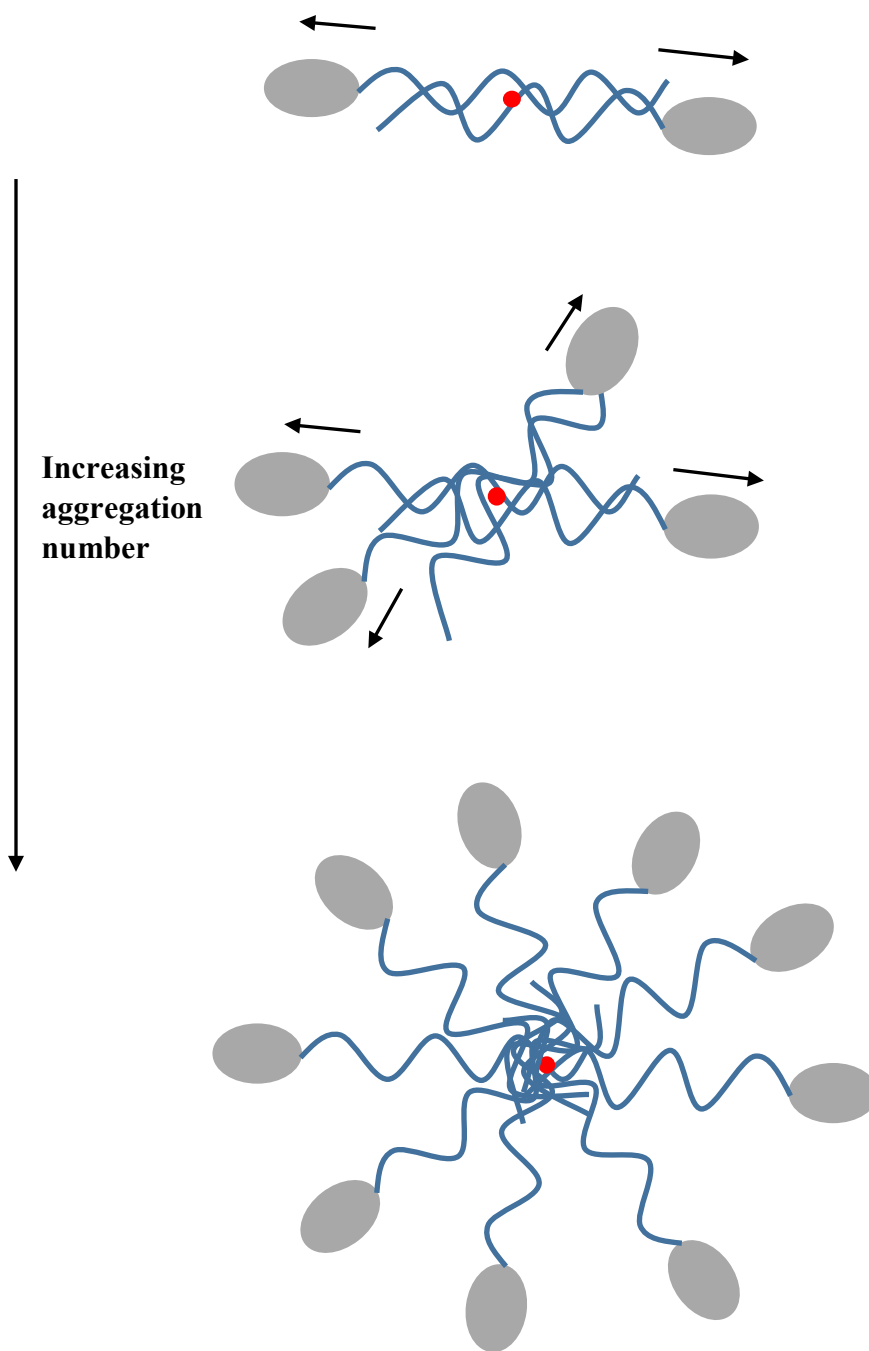


Figure 28: Schematic showing how inhibitor molecules move out from the center of mass to accommodate more molecules and ultimately form a perfect spherical micelle.

Imid-17 and Imid-10 have slightly different orientation of molecules in the clusters. This can be seen in Figure 29. The *rdf* show that terminal carbon of Imid-17 sees some water in the first solvation shell whereas this is not the case for Imid-10; in other words, for the same cluster aggregation number, tails in Imid-10 are a bit far away from the periphery relative to Imid-17. Also, both imid-17 and imid-10 clusters have the same R_g which means imid-17 clusters have a greater number density at the core (Figure 30), the packing is more efficient and interactions with water are reduced by wrapping around other alkyl tails (this is observed from visualizations). Interestingly, the number density at the periphery is also high for Imid-17 clusters (Figure 30), – this implies that the imidazolium rings are spread out at the periphery.

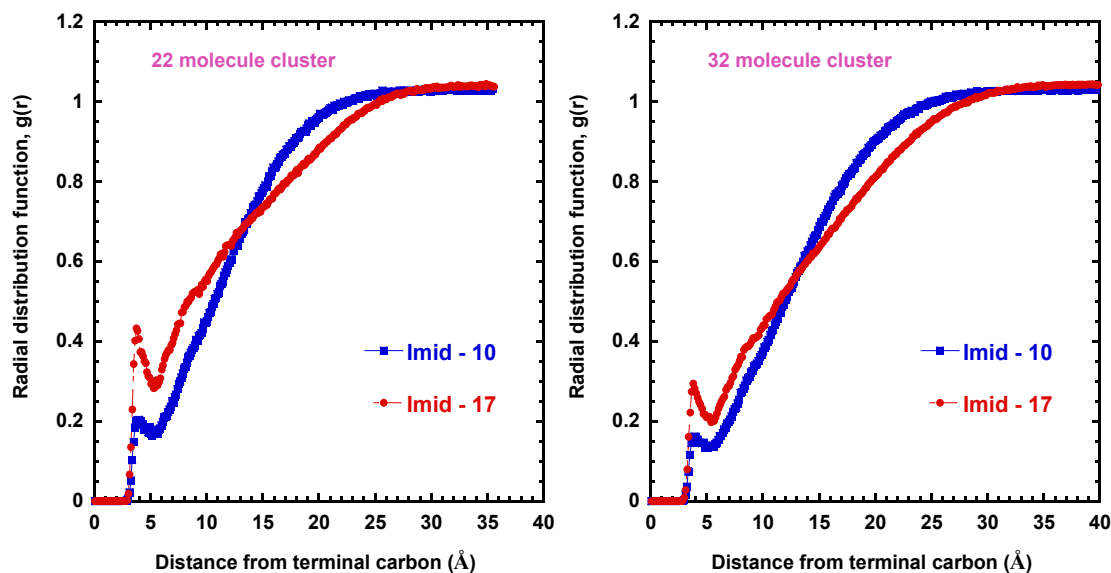


Figure 29: Radial distribution of water w.r.t. terminal carbon in alkyl tail, comparison between Imid-10 and Imid-17 clusters.

In summary, although the peripheral shape of the cluster is the same for both Imid-17 and Imid-10 clusters, the diffusion coefficient of imid-17 clusters is less than the imid-10 cluster because of the relatively high number density on the periphery and different orientation of molecules in Imid-17 clusters. The presence of a greater number of atoms at the periphery means more interactions with water molecules which is manifested as diminution of diffusion.

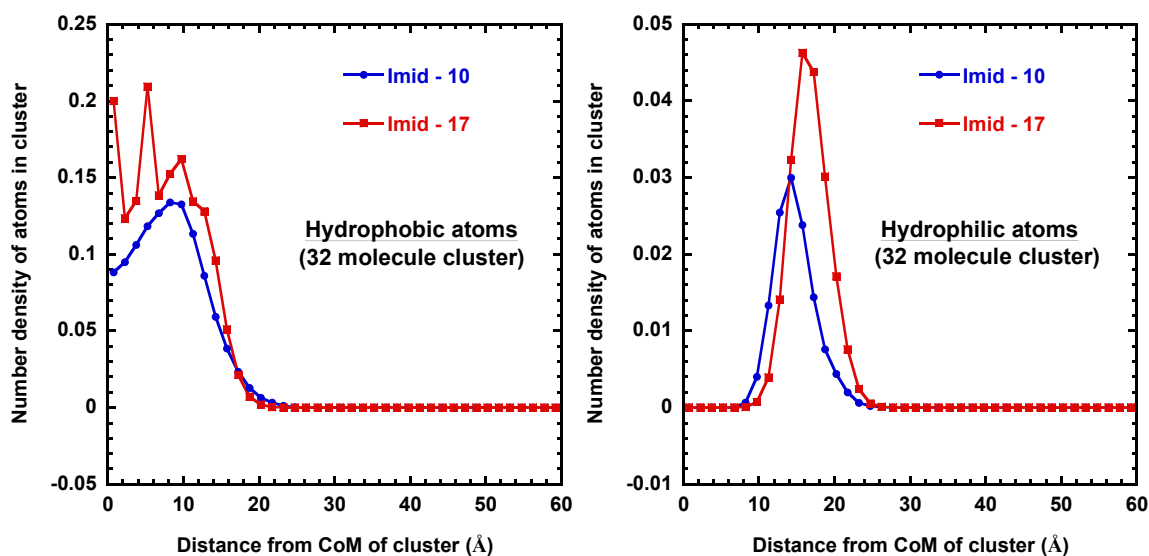


Figure 30: Radial distribution of hydrophobic and hydrophilic atoms w.r.t. center of mass of cluster, comparison of imid-17 & imid-10 clusters having 32 molecules.

4.2.1 Local Structure of the Liquid Using Radial Distribution Function, $g(r)$

The radial distribution function of water, $g_{OO}(r)$, shows two distinct peaks at 2.73\AA and 4.5\AA that represent first and second solvation shells (Figure 31). This data match with the data from the literature [65], [66]. Apart from water and inhibitor molecules, the simulation system has chlorides. The structure of inhibitor clusters are already discussed

in the previous section. Local structure near the chlorides is explored using *rdf*. Ions are known to get solvated in water as is evident from the peaks at 3.1Å & 4.83Å; in radial distribution function of water around chlorides, $g_{Cl-O}(\mathbf{r})$ (Figure 32). The data match with the Joung-Cheatham model that is used to simulate chlorides [58]. Since the inhibitor molecules carry net positive charge, it is expected that chlorides would diffuse to the clusters leading to their stabilization. This was explored by looking at the *rdf* of chlorides around the proton on the imidazoline ring (H^+), this proton is selected because it has the maximum positive partial charge on the polar group (Figure 32). A very strong peak is observed for $g_{H^+-Cl}(\mathbf{r})$ at 2.33Å (first solvation shell) and then it gradually decreases to the value of 1 at about 30Å (twice the R_g of the 32molecule cluster). Similar behavior is seen in other sizes of clusters. The gradual decrease in *rdf* is because of the presence of chlorides all around the clusters. Hence, it can be said that most of the chlorides are present near the inhibitor cluster stabilizing it and few chlorides are in the bulk solvated by water. This is in good accordance with the literature that, for ionic surfactants, micelle formation is favored in the presence of counter ions [67].

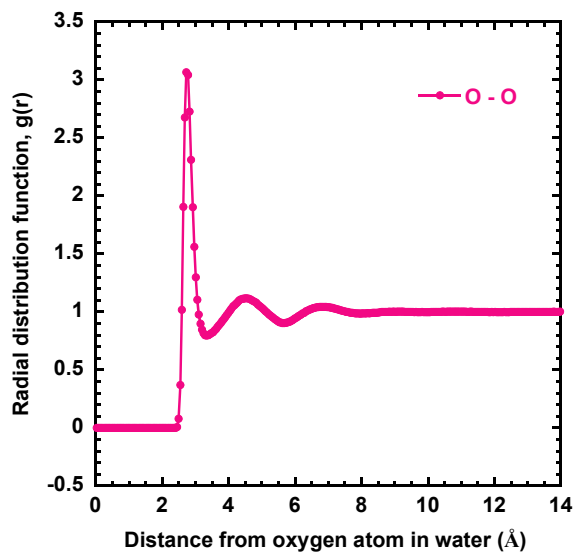


Figure 31: Radial distribution function, $g_{OO}(r)$, of SPC/E water.

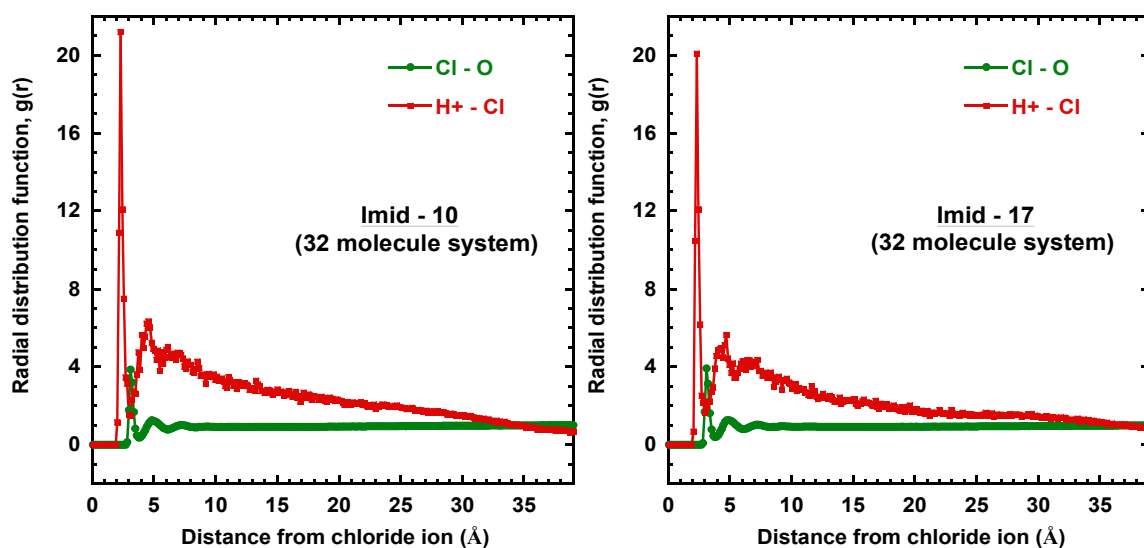


Figure 32: Radial distribution functions of chloride ions, $g_{H+-Cl}(r)$, & $g_{Cl-O}(r)$.

4.3 Free Energy Landscapes of Adsorption of an Inhibitor at Infinite Dilution

Simulation details for this study are given in section 3.5. As discussed in section 3.5, due to the presence of strongly adsorbed water layers on the metal surface, a free energy barrier is expected for adsorption of inhibitor on metal surfaces as the adsorbed

water layers need to be displaced. The free energy profile of adsorption for an inhibitor molecule in an infinite dilution system, simulation system has only one corrosion inhibitor and simulation box is big enough that it does not interact with its periodic images, was generated by considering ‘distance of center of mass of inhibitor from the metal surface’ to be the reaction coordinate. All the phase space along the reaction coordinate was sampled using umbrella sampling (technique described in section 3.2.4). The biased probability distribution from different umbrella sampling simulations are stitched together, an un-biased probability distribution is then generated using the weighted histogram analysis method, WHAM, described in section 3.2.5. The results obtained are presented and discussed in this section.

Figure 33 and Figure 34 show the biased histograms generated for Imid-10 and Imid-17, respectively, each curve in the graphs represent a biased simulation. Good overlap between the curves show that all the regions are well sampled. Many histograms are seen within a 5 Å distance from the metal surface. This region was difficult to sample because once the inhibitor (center of mass) enters this region, it is likely that the inhibitor has already displaced the water layers and is strongly attracted by the metal atoms. Multiple simulations were done with different force constants to ensure all regions along the reaction coordinate were sampled. Force constants used range from 10 kJ/mole to 120 kJ/mole. The spread along the x-axis and y-axis is different for curves because of the different force constants. This does not affect the free energy calculation as the applied bias is later removed in WHAM calculations. WHAM code implemented by Alan Grossfield [68] is used to calculate unbiased probability distribution.

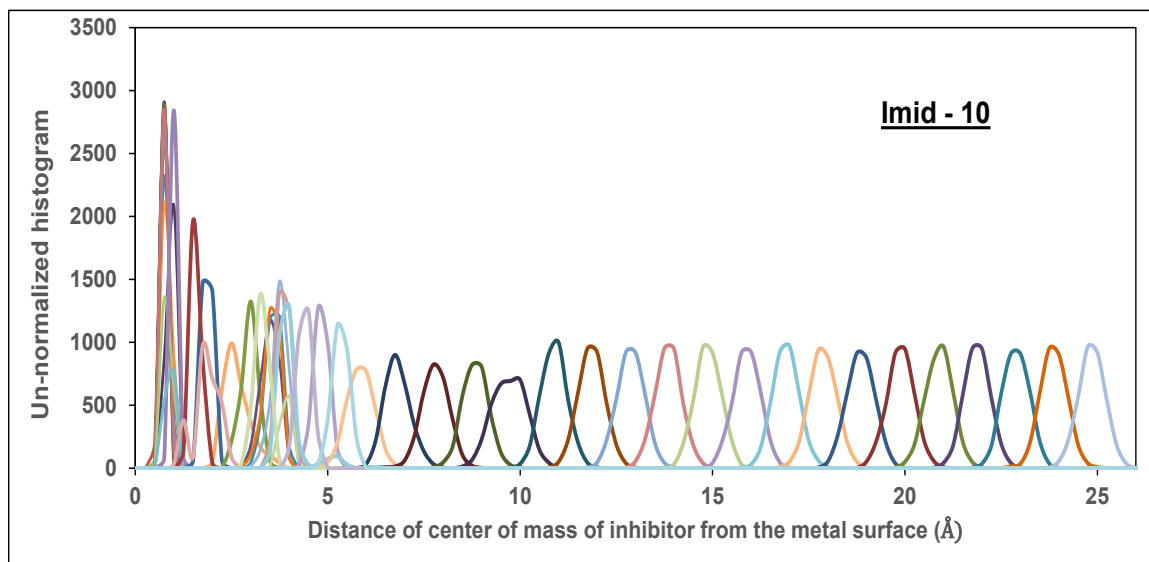


Figure 33: Histograms generated for Imid-10 by restraining the center of mass (of inhibitor) at different distances from the metal surface.

The free energy landscape calculated for Imid-10 & Imid-17 is shown in Figure 35. Free energy is represented in terms of thermal energy ($1 k_B T = 2.5 \text{ kJ/mole}$). Interestingly, there is no free energy barrier observed either for Imid-10 or Imid-17 to adsorb on the metal surface. A small peak seen at 5 \AA for Imid-10, $\sim(1.1 \pm 0.2)k_B T$, is not a free energy barrier as the required energy can be supplied by the thermal energy of the system itself. Both Imid-17 & Imid-10 have similar free energy profiles. The plateau region ($> 12 \text{ \AA}$) represent the bulk aqueous phase where the inhibitor molecule is not influenced by metal. Below 12 \AA , there is a moderate decrease in free energy until 7 \AA then free energy drops sharply.

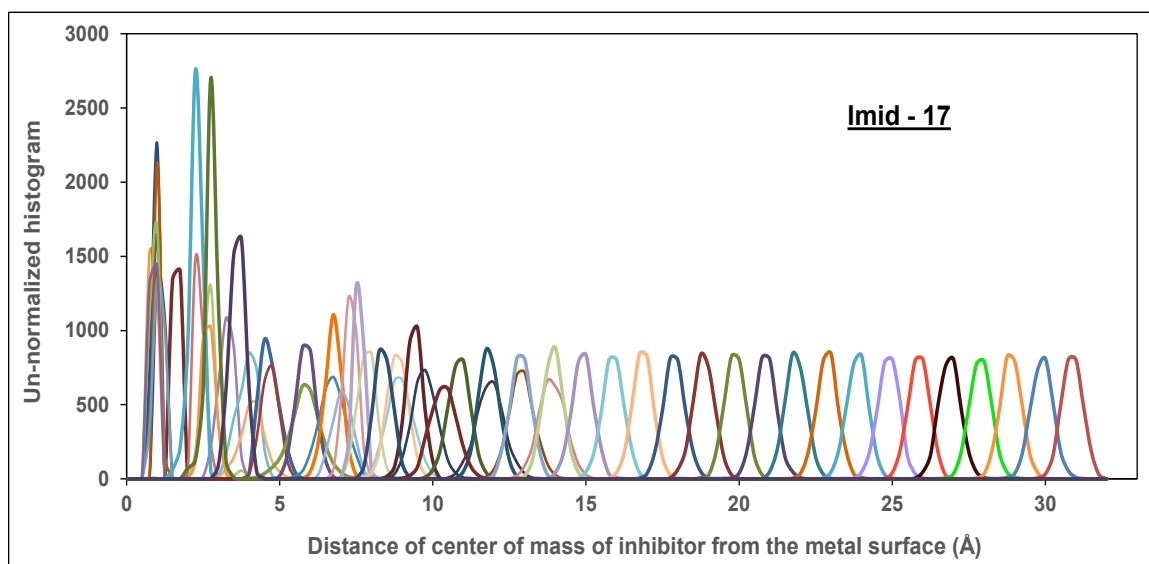


Figure 34: Histograms generated for Imid-17 by restraining the center of mass (of inhibitor) at different distances from the metal surface.

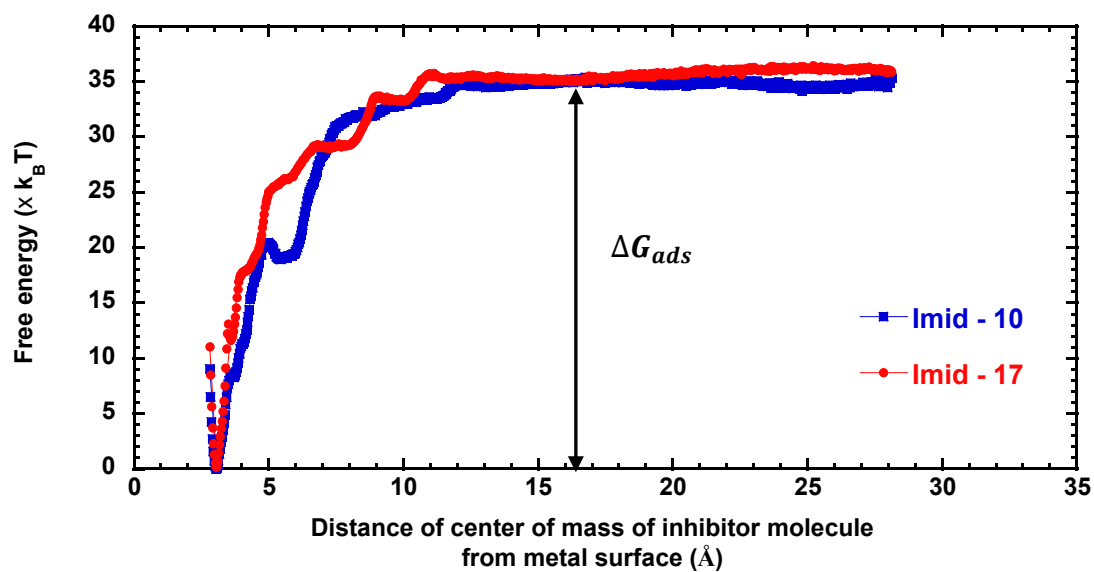


Figure 35: Free energy profile of Imid-10 and Imid-17 in an infinite dilution system; free energy is represented in terms of thermal energy ($1 k_B T = 2.5 kJ/mole$).

The decrease in free energy of the system is because of the additional interactions between inhibitor and metal atoms. The alkyl tail being hydrophobic is likely to displace water molecules on the surface; this could be the reason for slight difference in the slopes for the two profiles (Imid-17 being more hydrophobic displaces water more effectively and hence the higher slope). It is to be noted that, in these simulations there is no restraint on the orientation of the molecule and hence no comment can be made about the optimal orientation of adsorbed inhibitor with respect to the metal surface.

In order to calculate the change in free energy due to adsorption, one needs to define the ‘adsorbed’ and ‘non-adsorbed’ states. The length of alkyl tail in both inhibitor molecules is more than 10Å and the change in the free energy profile is significant below 10Å. As there is no free energy barrier observed, it is assumed that inhibitor interacts (adsorbs) with the metal atoms once its center of mass is within a 10Å distance from the metal surface. Therefore, all the configurations below 10Å are considered to be in an adsorbed state and above 10Å are considered non-adsorbed. Then free energy of adsorption is given by:

$$\Delta G_{ads} = -k_B T * \left(\ln \left(\sum_{i \in \xi \leq 10\text{\AA}} (P_i^u(\xi)) \right) - \ln \left(\sum_{j \in \xi > 10\text{\AA}} (P_j^u(\xi)) \right) \right) \quad (4.3)$$

Where, ‘ ξ ’ is the distance of center of mass of inhibitor molecule from the metal surface, and $P^u(\xi)$ is the unbiased probability distribution that is known from the WHAM calculations (Equation 3.15).

Similarly, enthalpy of adsorption is calculated using average total potential energy of adsorbed and non-adsorbed states. Enthalpy of adsorption is given by:

$$\Delta H_{ads} = \sum_{i \in \xi \leq 10\text{\AA}} \phi_i U_i - \sum_{i \in \xi > 10\text{\AA}} \phi_i U_i \quad (4.4)$$

Where U_i is the total potential energy of the microstate i , and ϕ_i is the normalized probability of system in microstate with energy U_i .

Change in entropy due to adsorption is calculated using Equation 4.5.

$$\Delta S_{ads} = \frac{\Delta H_{ads} - \Delta G_{ads}}{T} \quad (4.5)$$

Changes in adsorption free energy, enthalpy and entropy obtained for Imid-10 and Imid-17 are listed in Table 3.

Table 3: Free energy, enthalpy and entropy changes on adsorption in an infinite dilution system.

	Imid – 10	Imid -17
ΔG_{ads} (kJ/mole)	-75.16	-76.49
ΔH_{ads} (kJ/mole)	-143.11	-187.72
ΔS_{ads} (kJ/mole)	-0.23	-0.37

Imid-17 has a higher ΔH_{ads} as there are more interactions with the metal compared with Imid-10. Imid-17 loses more entropy because of the longer alkyl tail that makes a positive contribution to ΔG_{ads} . From Table 3, it is evident that the adsorption of a single inhibitor molecule is mainly driven by changes in enthalpy.

4.4 Free Energy Landscapes of Adsorption of an Inhibitor Cluster

NVT simulations of a metal–water system containing 32 inhibitor molecules showed rapid cluster formation in the bulk aqueous phase. An MD simulation is conducted

by bringing one of the clusters formed in the bulk to the metal surface (removed diffusion barrier) in anticipation of forming a self-assembled layer on the metal surface. Over the course of simulation, the cluster did not break/adsorb on the metal surface but diffused away into the bulk solution. The MD trajectory at different time instances is shown in Figure 36. The reason for this behavior is unknown, though it is likely that the inhibitor-inhibitor interactions present in the cluster are strong enough that any interaction with the metal surface does not break the cluster. Another interesting observation is that the cluster does not adsorb on the metal surface showing that there is a free energy barrier associated with adsorption. Hence, Free energy profiles for adsorption of clusters were subsequently generated using umbrella sampling.

An inhibitor cluster containing 19 molecules is considered for Imid-17 ($R_g \sim 12\text{\AA}$) and a cluster containing 18 molecules is considered for Imid-10 ($R_g \sim 11.4\text{\AA}$). The simulation set up is the same as that described in section 3.5, except for the presence of a cluster instead of a single molecule. The simulation box is big enough that it can be thought of as an inhibitor cluster present in an infinite dilution system. In these simulations, ‘distance between the metal surface and the center of mass of the cluster’ was considered as the reaction coordinate. The inhibitor cluster is initially placed far away from the surface ($> 60\text{\AA}$) and then slowly moved towards the desired reaction coordinate by applying harmonic bias potential.

$$V_i(\xi) = \frac{1}{2}k(\xi - \xi_i)^2 \quad (4.6)$$

Where k is the force constant, ξ is the reaction coordinate (distance between metal surface and center of mass of the cluster) and ξ_i is the desired reaction coordinate for the i^{th} window. For this sampling, the force constant chosen is 5 kcal/mol.

The cluster was monitored throughout the simulations to ensure that the cluster is intact. Free energy profiles generated for adsorption of Imid-17 and Imid-10 clusters are shown in Figure 37 and Figure 38, respectively.

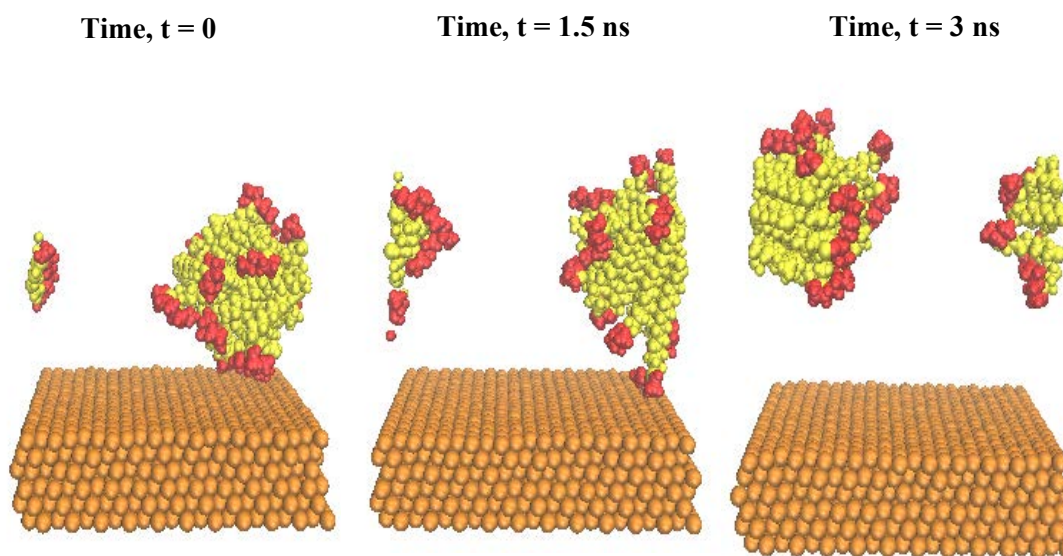


Figure 36: MD trajectory of an NVT simulation that has a single cluster of imid-17 inhibitors near the metal surface; orange represent metal (Au) atoms, red represents atoms on hydrophilic head groups and yellow represents hydrophobic alkyl tails. (chlorides and water are not shown for simplicity).

Figure 37 show that free energy of the system is lowest when the center of mass of the cluster is at 16Å away from the metal surface. This refers to the configuration in which the cluster removed the water molecules and is adsorbed to the metal surface. Free energy

in the bulk water, where there is no interaction with metal, is $2.7k_B T$ times more. Interestingly, there is a peak observed between 16\AA and the bulk water at 21\AA , *i.e.*, an external energy of $7.3k_B T$ needs to be supplied to the system to bring an Imid-17 cluster from the bulk to the surface of the metal. For a uniformly distributed solid sphere, the radius is $\sqrt{\frac{5}{3}}$ times the root mean squared radius of gyration (Rg); consequently, the radius of the Imid-17 cluster is 15.5\AA which implies that the cluster interacts with the adsorbed water layers when its center of mass is at 21\AA . The peak seen is associated with the energy required to disrupt/displace the adsorbed layers of water.

Figure 38 show that the free energy of the Imid-10 cluster system is lowest when the center of mass of the cluster is in the bulk water ($> 34\text{\AA}$), where the metal has no interaction with the inhibitors. As the inhibitor cluster comes closer to the surface, there is an increase in free energy of the system that reaches a maximum at 21\AA then further decreases until a distance of 15\AA is reached. Below 15\AA , there is a sharp increase in free energy of the system suggesting that the center of mass of a cluster cannot go further towards the metal. One evident observation is that the Imid-10 cluster has to climb over a free energy barrier of $7.3k_B T$ to move from bulk phase to an adsorbed state. The Rg of the Imid-10 cluster is 11.4\AA which means the radius of the cluster is 14.7\AA . Similar to the postulate for Imid-17, the peak in the free energy profile corresponds to the energy required to disrupt the adsorbed water layers. However, the adsorbed state (at 15\AA) is a metastable state for the Imid-10 cluster which means they are thermodynamically more stable in the bulk aqueous phase.

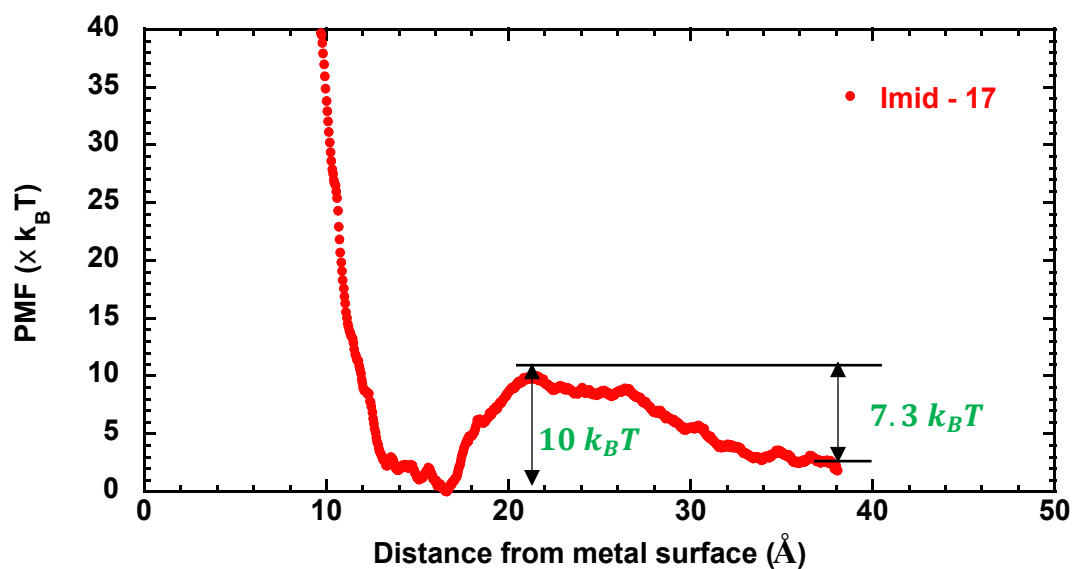


Figure 37: Free energy profile of adsorption of Imid-17 cluster (19 molecules) on a Au metal surface.

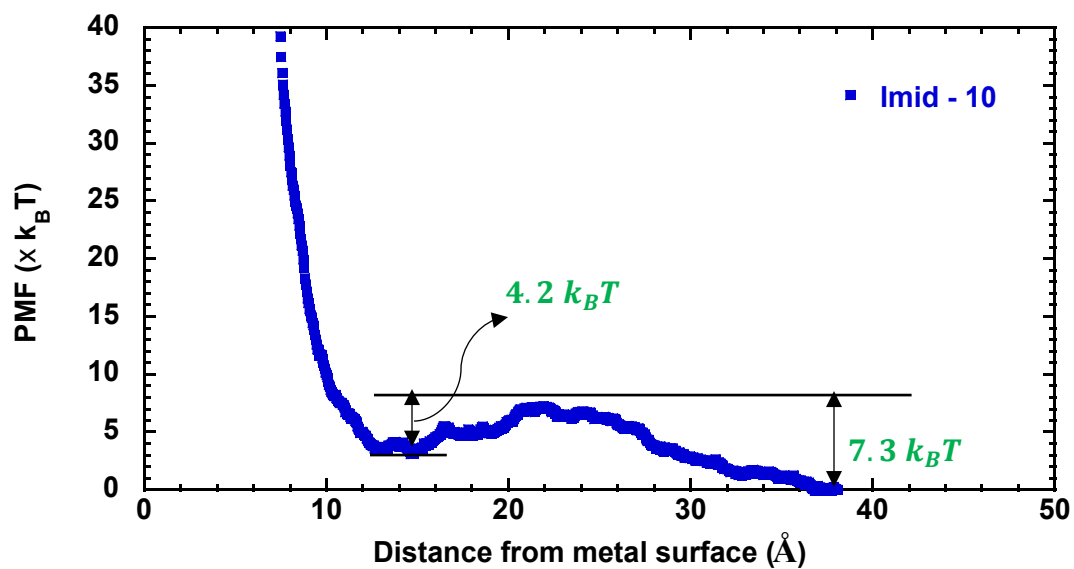


Figure 38: Free energy profile of adsorption of Imid-10 cluster (18 molecules) on a Au metal surface.

In both the systems, an increase in free energy is observed when center of mass of the cluster is below 15Å from the metal surface. This could either be associated with deformation of the cluster shape (to bring down the center of mass) or disruption of the adsorbed water. Visualizations of the biased simulations ($\xi < 15\text{\AA}$) show that few inhibitor molecules in the cluster are in contact with the metal surface while there is still a water layer present between the cluster and metal surface (Figure 39 & Figure 40). Also, the cluster is observed to flatten in the XY plane for both Imid-10 and Imid-17. From this data, the reason for increase in free energy is not clear. In order to study the system at its minimum free energy state, a few simulations were conducted in the range $12 < \xi < 18$ without the umbrella sampling bias. The cluster in these simulations is expected to sample the minimum in the free energy profile. Visualizations from these simulations show that at the minimum in the free energy, the cluster is in contact with the metal surface and it has regained its spherical shape (Figure 42). Therefore, the free energy barrier of 18 kJ/mole is associated with the removal of adsorbed water layers while the increase in free energy below 15Å is associated with the deformation of the cluster.

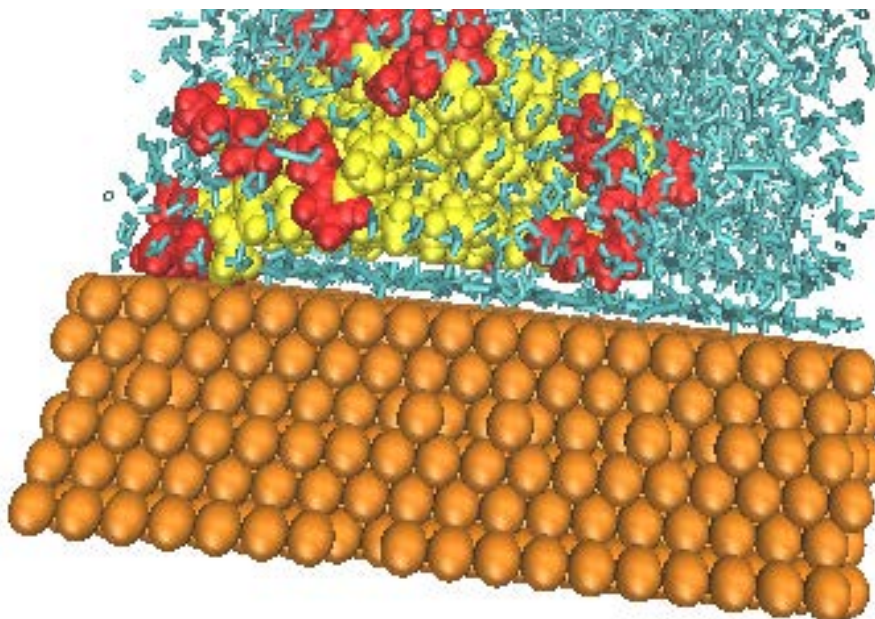


Figure 39: Snapshot of the Imid-17 cluster when the center of mass of cluster is biased at 11\AA from the metal surface. Chlorides not shown for simplicity.

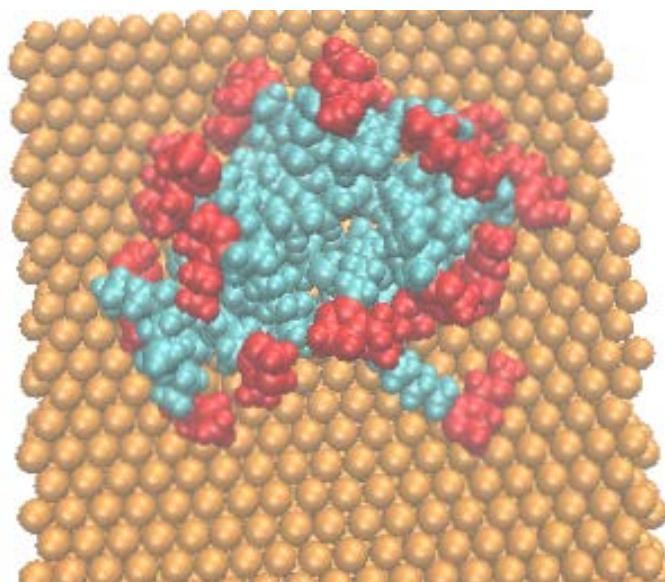


Figure 40: Snapshot of the Imid-10 cluster (plane view) when the center of mass of the cluster is biased at 10\AA from the metal surface. Water not shown for simplicity; red represents hydrophilic head group while cyan represents the hydrophobic tails.

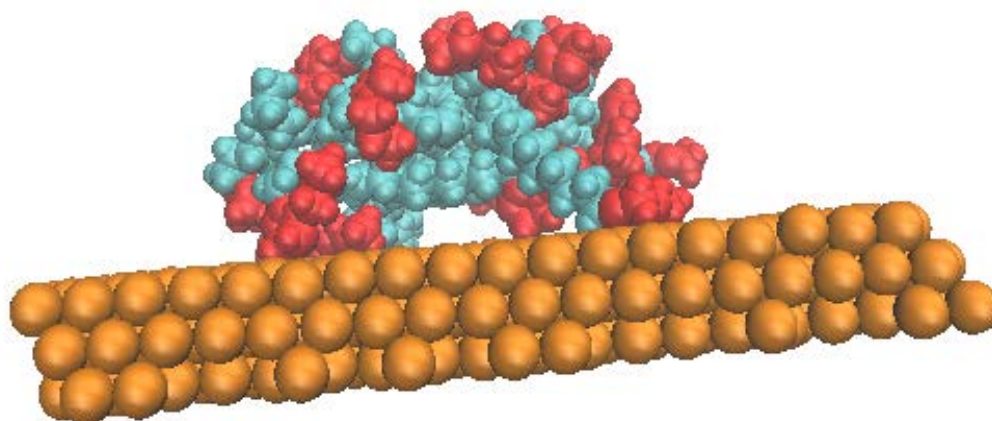


Figure 41: Side view of the Imid-10 cluster shown in Figure 40.

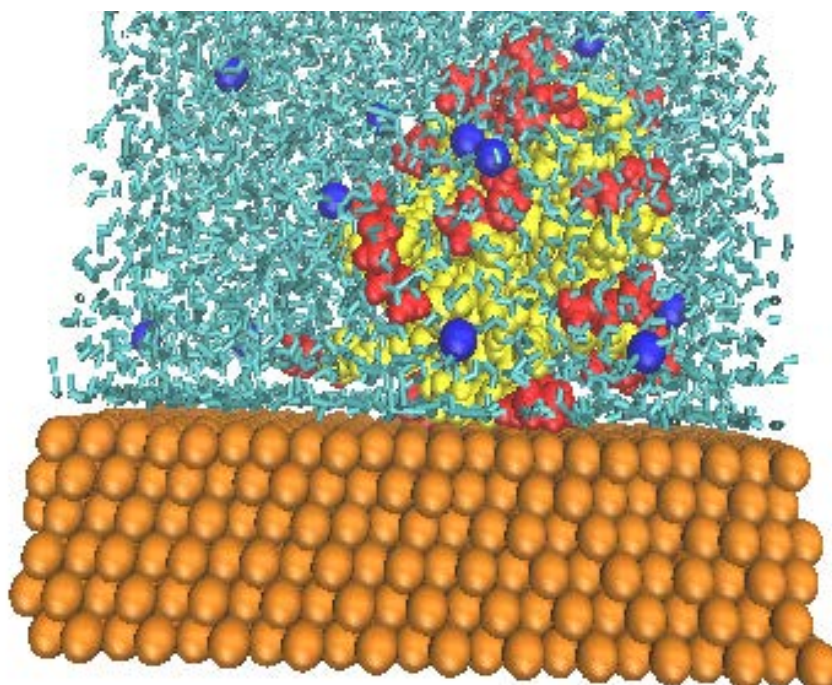


Figure 42: Minimum free energy state for an Imid-17 cluster; snapshot taken from an unbiased simulation. Blue represents chlorides, yellow represents alkyl tails and red represent polar head groups.

5 CONCLUSIONS & FUTURE WORK

5.1 Summary of Results

In this study, free energy barriers of adsorption, and diffusion characteristics of different aggregates formed by two imidazolinium-type corrosion inhibitors of different alkyl tail lengths have been computed using atomistic simulations. The diffusion results were compared with those calculated using the theoretical Stokes-Einstein relations. It was found that imidazolinium-type corrosion inhibitors form spherical micelles with their hydrophilic groups on the periphery and hydrophobic alkyl tails huddled in the core of the cluster. Molecules with longer alkyl tails pack more efficiently in the cluster and thus have higher number density, both at the periphery and at the core. This led to a different diffusion coefficient despite the fact that cluster formed by both inhibitor molecules have the same radius of gyration.

There is no free energy barrier involved in the adsorption of Imid-17 and Imid-10 as single molecules (in infinite dilution systems) on an Au metal surface. If the diffusion barrier is removed, the inhibitor molecules adsorb spontaneously on the metal surface. Also, free energy of adsorption is the same, -76 kJ/mole, for both inhibitor molecules. The adsorption process is primarily driven by changes in enthalpy.

When micelles form in the aqueous phase, in addition to the diffusion barrier, a large free energy barrier of $7.3k_B T$ is involved in the adsorption of micelles on the Au metal surface. Although the energy barrier is the same for both Imid-17 and Imid-10 clusters, adsorption of the Imid-10 cluster results in a metastable state whilst Imid-17 clusters form a thermodynamically more favorable state. The adsorption barrier is due to

the inability of the clusters to remove the adsorbed water layers on the metal surface, a possible reason being the unavailability of hydrophobic tails. Overall, the free energy calculations suggest that avoiding micelle formation in the bulk would result in spontaneous and better adsorption.

5.2 Future Work

Suggested topics to expand upon the research described in this thesis are as follows:

- In the work described herein, only one inhibitor cluster having 19 molecules is sampled. The free energy barrier observed is attributed to the inhibitor-inhibitor interactions that exist in the cluster. The higher the aggregation number, the greater the inhibitor-inhibitor interactions. Therefore, not all clusters are expected to have the same adsorption barrier. It will be useful to explore the effect of cluster size on adsorption energy barriers. A working hypothesis will be that there is an optimal cluster size below which there is no free energy barrier for adsorption.
- Metal atoms are modeled as neutral LJ atoms. The existence of partial charge on the metal atoms will likely affect the density profile of water at the interface, and hence, the free energy of adsorption. Umbrella sampling in the presence of a charged metal would be useful.
- In the present work, critical aggregation numbers are not reached for either Imid-17 or Imid-10. Generally, micelles are formed in the system by aggregation of smaller sized clusters. As discussed, ionic surfactants have an electrical double layer on their periphery that creates resistance against two clusters to join. Factors

affecting/assisting the formation of micelles are worth exploring relating to diffusion, adsorption and corrosion inhibition.

- Simulation work should be extended to cover additional molecular variants of imidazolinium-type inhibitors, as well as amphiphilic surfactant molecules such as quaternary ammonium, phosphate ester and pyridinium compounds.

REFERENCES

- [1] "Corrosion cost and preventive strategies in the United States," NACE, 2002.
- [2] "International measures of prevention, application, and economics of corrosion technologies study," (IMPACT) NACE, 2013.
- [3] P. Roberge, "Corrosion Inhibitors," in *Handbook of Corrosion Engineering*, McGraw-Hill, 2000.
- [4] I. B. Obot, "Recent advances in computational design of organic materials for corrosion protection of steel in aqueous media," in *Developments in corrosion protection*, InTech, 2014.
- [5] S. Papavinas, "Evaluation and selection of corrosion inhibitors," in *Uhlig's Corrosion Handbook*, John Wiley & Sons, 1999.
- [6] T. Libin, X. Li, L. Li, G. Mu and G. Liu, "Interfacial behavior of 4-(2-pyridylazo) resorcin between steel and hydrochloric acid," *Surface and Coatings Technology*, vol. 201, no. 1, pp. 384 - 388, 2006.
- [7] N. C. Subramanyam, B. S. Sheshadri and S. M. Mayanna, "Thiourea and substituted thioureas as corrosion inhibitors for aluminium in sodium nitrite solution," *Corrosion Science*, vol. 34, no. 4, pp. 563 - 571, 1993.
- [8] O. Oliveres, N. V. Likhanova, B. Gomez, J. Navarrete, Llanos-Serrano, E. Arce and J. M. Hallen, "Electrochemical and XPS studies of decylamides of amino acids adsorption on carbon steel in acidic environment," *Applied Surface Science*, vol. 252, no. 8, pp. 2894 - 2909, 2006.
- [9] E. Umit, D. Yuzer and K. C. Emregul, "The inhibitory effect of bis-2,6-(3, 5-dimethylpyrazolyl) pyridine on the corrosion behavior of mild steel in HCl solution," *Materials Chemistry and Physics*, vol. 109, no. 2, pp. 492 - 499, 2008.
- [10] N. Ehteram, "Evaluation of inhibitive action of some quaternary N-heterocyclic compounds on the corrosion of Al-Cu alloy in hydrochloric acid," *Materials Chemistry and Physics*, vol. 114, no. 2, pp. 533 - 541, 2009.
- [11] J. Cruz, R. Martinez, J. Gnesca and E. Garcia-Ochoa, "Experimental and theoretical study of 1-(2-ethylamino)-2-methylimidazoline as an inhibitor of carbon steel corrosion in acid media," *Journal of Electroanalytical Chemistry*, vol. 566, no. 1, pp. 111 - 121, 2004.

- [12] S. Ramachandran, R. Bao-Liang, B. Mario, C. Huey, T. Yongchum and G. A. William, "Self-assembled monolayer mechanism for corrosion inhibition of iron by imidazolines," *Langmuir*, vol. 12, no. 26, pp. 6419 - 6428, 1996.
- [13] A. Edwards, C. Osborne, S. Webster, D. Klenerman, M. Joseph, P. Ostovar and M. Doyle, "mechanistic studies of the corrosion inhibitor oleic imidazoline," *Corrosion Science*, vol. 36, no. 2, pp. 315 - 325, 1994.
- [14] C. D. Taylor, "Modeling corrosion, atom by atom," *The Electrochemical Society Interface*, vol. 23, no. 4, pp. 59 - 64, 2014.
- [15] Z. Jun, G. Qiao, S. Hu, Y. Yan, Z. Ren and L. Yu, "Theoretical evaluation of corrosion inhibition performance of imidazoline compounds with different hydrophilic groups," *Corrosion Science*, vol. 53, no. 1, pp. 147 - 152, 2011.
- [16] M. G. V. Satyanarayana, V. Himabindu, Y. Kalpana, R. K. Muttineni and K. Kumar, "Part 1: In-silico studies as corrosion inhibitor and its experimental investigation on mild steel in wet-lab," *Journal of Molecular Structure: THEOCHEM*, vol. 912, no. 1, pp. 113 - 118, 2009.
- [17] J. Vosta and J. Eliasek, "Study on corrosion inhibition from aspect of quantum chemistry," *Corrosion Science*, vol. 11, no. 4, pp. 223 - 229, 1971.
- [18] W. Durnie, R. De Marco, A. Jefferson and B. Kinsella, "Development of a structure-activity relationship for oil field corrosion inhibitors," *Journal of the Electrochemical Society*, vol. 146, no. 5, pp. 1751 - 1756, 1999.
- [19] W. Durnie, R. De Marco, B. Kinsella, A. Jefferson and B. Pejic, "Predicting the adsorption properties of carbondioxide corrosion inhibitors using a structure-activity relationship," *Journal of the Electrochemical Society*, vol. 152, no. 1, pp. B1 - B11, 2005.
- [20] E. E. Ebenso, T. Arslan, F. Kandemirli, Love I, C. Ogretir, M. Saracoglu and S. A. Umoren, "Theoretical studies of some sulphonamides as corrosion inhibitors for mild steel in acidic medium," *International Journal of Quaantrum Chemistry*, vol. 110, no. 14, pp. 2614 - 2636, 2010.
- [21] K. F. Khaled, "Monte Carlo simulations of corrosion inhibition of mild steel in 0.5M sulphuric acid by some green corrosion inhibitors," *Journal of Solid State Electrochemistry*, vol. 13, no. 11, pp. 1743 - 1756, 2009.

- [22] K. F. Khaled, "Molecular simulation, quantum chemical calculations and electrochemical studies for inhibition of mild steel by triazoles," *Electrochimica Acta*, vol. 53, no. 9, pp. 3484 - 3492, 2008.
- [23] A. Motta, M. P. Gaigeot and D. Costa, "AIMD evidence of inner sphere adsorption of glycine on a stepped (101) boehmite AlOOH surface," *The Journal of Physical Chemistry C*, vol. 116, no. 44, pp. 23418 - 23427, 2012.
- [24] M. G. Fontana, Corrosion engineering, Tata McGraw-Hill, 2005.
- [25] C. G. Dariva and A. F. Galio, "Corrosion inhibitors - principles, mechanisms and applications," in *Developments in Corrosion protection*, Intech, 2014.
- [26] Y. Duda, R. Govea-Rueda, M. Galicia, H. I. Beltran and L. S. Zamudio-Rivera, "Corrosion inhibitors: design, performance and computer simulations," *The Journal of Physical Chemistry B*, vol. 109, no. 47, pp. 22674 - 22684, 2005.
- [27] A. Y. El-Etre, M. Abdallah and Z. E. El-Tantawy, "Corrosion inhibition of some metals using lawsonia extract," *Corrosion Science*, vol. 47, no. 2, pp. 385 - 395, 2005.
- [28] R. M. Palou, O. Olivares-Xomelt and N. V. Likhanova, "Environmentally friendly corrosion inhibitors," in *Developments in corrosion protection*, InTech, 2014.
- [29] E. McCafferty, Introduction to corrosion science, Springer Science & Business Media, 2010.
- [30] D. Wang, S. Li, Y. Ying, M. Wang, H. Xiao and Z. Chen, "Theoretical and experimental studies of structure and inhibition efficiency of imidazoline derivatives," *Corrosion Science*, vol. 41, no. 10, pp. 1911 - 1919, 1999.
- [31] V. S. Sastri, Corrosion inhibitors: principles and applications, John Wiley, 1998.
- [32] Y. J. Tan, S. Bailey and B. Kinsella, "An investigation of formation and destruction of corrosion inhibitor films using electrochemical impedance spectroscopy (EIS)," *Corrosion Science*, vol. 38, no. 9, pp. 1545 - 1561, 1996.
- [33] A. A. Al-Amiery, A. H. Kadhum, A. H. M. Alobaidy, A. B. Mohamad and P. S. Hoon, "Novel corrosion inhibitor for mild steel in HCl," *Materials*, vol. 7, no. 2, pp. 662 - 672, 2014.
- [34] G. Gao and C. H. Liang, "1, 3-Bis-diethylamino-propan-2-ol as volatile corrosion inhibitor for brass," *Corrosion Science*, vol. 49, no. 9, pp. 3479 - 3493, 2007.

- [35] A. Domenicano and I. Hargittai, *Accurate molecular structures: their determination and importance*, Oxford University Press, 1992.
- [36] N. Hackerman, "Recent advances in understanding of organic inhibitors," *Corrosion*, vol. 18, no. 9, pp. 332 - 337, 1962.
- [37] W. J. Lorenz and F. Mansfeld, "Interface and interphase corrosion inhibition," *Electrochimica Acta*, vol. 31, no. 4, pp. 467 - 476, 1986.
- [38] N. Pebere, M. Duprat, F. Dabosi, A. Lattes and A. De Saignac, "Corrosion inhibition study of a carbon steel in acidic media containing hydrogen sulphide and organic surfactants," *Journal of Applied Electrochemistry*, vol. 18, no. 2, pp. 225-231, 1988.
- [39] C. Cao, "On electrochemical techniques for interface inhibitor research," *Corrosion Science*, vol. 38, no. 12, pp. 2073 - 2082, 1996.
- [40] C. D. Taylor, C. Ashwini, J. Vera and N. Sridhar, "A multiphysics perspective on mechanistic models for chemical corrosion inhibitor performance," *Journal of the Electrochemical Society*, vol. 162, no. 7, pp. C369 - C375, 2015.
- [41] M. L. Free, "Understanding the effect of surfactant aggregation on corrosion inhibition of mild steel in acidic medium," *Corrosion Science*, vol. 44, no. 12, pp. 2865 - 2870, 2002.
- [42] A. Vishnyakov, M. T. Lee and A. V. Neimark, "Prediction of the critical micelle concentration of nonionic surfactants by dissipative particle dynamics simulations," *The Journal of Physical Chemistry letters*, vol. 4, no. 5, pp. 797 - 802, 2013.
- [43] C. D. Taylor, C. Ashwini, J. Vera and N. Sridhar, "Design and prediction of corrosion inhibitors from quantum chemistry ii. A general framework for prediction of effective oil/water partition coefficients and speciation from quantum chemistry," *Journal of the Electrochemical Society*, vol. 162, no. 7, pp. C347 - C353, 2015.
- [44] C. Li, S. Richter and S. Nestic, "Effect of corrosion inhibitor on water wetting and CO₂ corrosion in an oil-water two-phase system," in *17th International Corrosion Congress*, 2008.
- [45] S. K. Mondal and S. R. Taylor, "The identification and characterization of organic corrosion inhibitors: correlation of a computational model with experimental results," *Journal of the Electrochemical Society*, vol. 161, no. 10, pp. C476 - C485, 2014.

- [46] Y. Xiong, B. Brown, B. Kinsella, S. Nestic and A. Pailleret, "Atomic force microscopy study of the adsorption of surfactant corrosion inhibitor films," *Corrosion*, vol. 70, no. 3, pp. 247 - 260, 2013.
- [47] C. Y. Chao, L. F. Lin and D. D. Macdonald, "A point defect model for anodic passive films I. Film growth kinetics," *Journal of the Electrochemical Society*, vol. 128, no. 6, pp. 1187 - 1194, 1981.
- [48] C. D. Taylor, S. A. Wasileski, J. S. Filhol and M. Neurock, "First principles reaction modeling of the electrochemical interface: Consideration and calculation of a tunable surface potential from atomic and electronic structure," *Physical Review B*, vol. 73, no. 16, p. 165402, 2006.
- [49] L. G. Qiu, Y. Wu, Y. M. Wang and X. Jiang, "Synergistic effect between cationic gemini surfactant and chloride ion for the corrosion inhibition of steel in sulphuric acid," *Corrosion Science*, vol. 50, no. 2, pp. 576 - 582, 2008.
- [50] M. P. Allen and D. J. Tildesley, *Computer simulation of liquids*, Oxford University Press, 2017.
- [51] J. Kastner, "Umbrella sampling," *Wiley Interdisciplinary Reviews: Computational Molecular Science*, vol. 1, no. 6, pp. 932 - 942, 2011.
- [52] S. Kumar, J. M. Rosenberg, D. Bouzida, R. H. Swendsen and P. A. Kollman, "The weighted histogram analysis method for free-energy calculations on biomolecules. I. The method," *Journal of Computational Chemistry*, vol. 13, no. 8, pp. 1011 - 1021, 1992.
- [53] A. M. Ferrenberg and R. H. Swendsen, "New monte carlo technique for studying phase transitions," *Physical Review Letters*, vol. 61, no. 23, p. 2635, 1988.
- [54] A. M. Ferrenberg and R. H. Swendsen, "Optimized monte carlo data analysis," *Physical Review Letters*, vol. 63, no. 12, p. 1195, 1989.
- [55] A. Radenovic, *Brownian motion and single particle tracking*, Advanced Bioengineering method laboratory, Ecole polytechnique federal de Lausanne, 2014.
- [56] H. Arkin and W. Janke, "Gyration tensor based analysis of the shapes of polymer chains in an attractive spherical cage," *The Journal of Chemical Physics*, vol. 138, no. 5, p. 054904, 2013.

- [57] J. Wang, R. M. Wolf, J. W. Caldwell, P. A. Kollman and D. A. Case, "Development and testing of a general amber force field," *Journal of Computational Chemistry*, vol. 25, no. 9, pp. 1157 - 1174, 2004.
- [58] I. S. Joung and T. E. Cheatham III, "Molecular dynamics simulations of the dynamic and energetic properties of alkali and halide ions using water-model-specific ion parameters," *The Journal of Physical Chemistry B*, vol. 113, no. 40, pp. 13279 - 13290, 2009.
- [59] H. J. C. Berendsen, J. R. Grigera and T. P. Straatsma, "The missing term in effective pair potentials," *Journal of Physical Chemistry*, vol. 91, no. 24, pp. 6269 - 6271, 1987.
- [60] W. G. Hoover, "Canonical dynamics: equilibrium phase-space distributions," *Physical Review A*, vol. 31, no. 3, p. 1695, 1985.
- [61] W. A. Hoover, "Constant-pressure equations of motion," *Physical Review A*, vol. 34, no. 3, p. 2499, 1986.
- [62] S. Plimpton, "Fast parallel algorithms for short-range molecular dynamics," *Journal of Computational Physics*, vol. 117, no. 1, pp. 1 - 19, 1995.
- [63] H. Heinz, T. J. Lin, R. Kishore Mishra and F. S. Emami, "Thermodynamically consistent force fields for the assembly of inorganic, organic and biological nanostructures: the INTERFACE force field," *Langmuir*, vol. 29, no. 6, pp. 1754 - 1765, 2013.
- [64] H. Heinz, R. A. Vaia, B. L. Rarner and R. R. Naik, "Accurate simulation of surfaces and interfaces of face-centered cubic metals using 12-6 and 9-6 Lennard-Jones potentials," *The Journal of Physical Chemistry C*, vol. 112, no. 44, pp. 17281 - 17290, 2008.
- [65] P. Mark and L. Nilsson, "Structure and dynamics of TIP3p, SPC and SPC/E water models at 298K," *The Journal of Physical Chemistry A*, vol. 105, no. 43, pp. 9954 - 9960, 2001.
- [66] A. K. Soper, "The radial distribution functions of water and ice from 220 to 673 K and at pressures upto 400 MPa," *Chemical Physics*, vol. 258, no. 2, pp. 121 - 137, 2000.
- [67] J. C. Berg, *An introduction to interfaces & colloids: the bridge to nanoscience*, World Scientific, 2010.

- [68] A. Grossfield, "WHAM: the weighted histogram analysis method, version 2.0.9.1," <http://membrane.urmc.rochester.edu/content/wham>.



OHIO
UNIVERSITY

Thesis and Dissertation Services